UNIVERSITAT POLITÈCNICA DE CATALUNYA
BARCELONATECH
Escola d'Enginyeria de Barcelona Est

MASTER FINAL THESIS

Màster en Ciència i Enginyeria de Materials

VIBRATION ASSISTED BALL BURNISHING FOR 720 NICKEL ALLOY

Report and Annexes

Author: Victoria Plana García
Supervisor: Toni Travieso Rodríguez
Co-Supervisor: Jordi Llumà Fuentes

Announcement: June 2020

Resum

En aquest treball de final de màster s'analitza l'efecte del procés de brunyit amb bola assistit per vibracions sobre la textura d'una superfície plana prèviament fresada de l'aliatge 720 base níquel. Es tracta d'un material de gran rellevància en el desenvolupament de peces clau a la industria aeronàutica. L'anàlisi es centra en la possible influència de diversos factors del procés com: la força de precàrrega, el número de passades realitzades, la velocitat lineal de l'eina, la topologia de la superfície inicial i l'estratègia seguida per a combinar l'ordre i direcció de les diferents passades. Per a poder estudiar l'efecte de tots aquests factors, s'aplica un disseny d'experiments optimitzat per a minimitzar el número d'assajos necessaris.

L'adquisició de dades experimentals es realitza mitjançant un sensor òptic topogràfic y es tracten posteriorment amb un software especialitzat que calcula els diversos paràmetres que caracteritzen la superfície. La discussió dels resultats, que conté diversos estudis estadístics ANOVA, es centra en l'efecte el brunyit sobre: la reducció de la textura, la redistribució del material i la possible reorientació de de l'anisotropia superficial. A més, es comparen els resultats quan el brunyit es realitza amb i sense l'assistència de vibracions.

Finalment, es conclou la combinació de factors que resulta en una millor topografia superficial i s'estableixen els següents passos recomanats per a aquesta línia d'investigació.

Resumen

En este trabajo de final de máster se analiza el efecto del proceso de bruñido con bola asistido por vibraciones sobre la textura de una superficie plana previamente fresada de la aleación 720 base níquel. Se trata de un material de gran importancia en el desarrollo de piezas clave de la industria aeronáutica. El análisis se centra en la posible influencia de diversos factores del proceso como: la fuerza de la precarga, el número de pasadas realizadas, la velocidad lineal de la herramienta, la topología de la superficie inicial y la estrategia seguida para combinar el orden y dirección de las distintas pasadas. Para poder estudiar el efecto de todos estos factores, se aplica un diseño de experimentos optimizado para minimizar el número de ensayos necesarios.

La adquisición de datos experimentales se realiza mediante un sensor óptico topográfico y se tratan posteriormente con un software especializado que calcula los diversos parámetros que caracterizan a la superficie. La discusión de los resultados, la cual engloba diversos estudios estadísticos mediante ANOVA, se centra en el efecto que tiene el bruñido sobre: la reducción de la textura, la redistribución del material y la posible reorientación de la anisotropía de la superficie. Además, se comparan los resultados cuando el bruñido se realiza con y sin la asistencia de vibraciones.

Finalmente, se concluye con la combinación de factores que lleva a una mejor topografía superficial y se establecen los siguientes pasos recomendados para esta línea de investigación.

Abstract

In this master final thesis, the effect of the vibration-assisted ball burnishing process on the texture of a previously milled flat surface of 720 nickel alloy is analysed. It is a material of great importance in the development of key parts in the aeronautical industry. The analysis focuses on the possible influence that five factors of the process may have: the preload force, the number of passes, the linear speed of the tool, the topology of the initial surface and the strategy followed to combine the order and direction of the different passes. In order to study the effect of all these factors, an optimised design of experiments is applied to minimize the number of tests required.

The acquisition of experimental data is carried out using a topographic optical sensor and are subsequently treated with specialised software that calculates the parameters that characterise the surface. The discussion of the results, which includes various statistical studies using ANOVA, focuses on the effect of burnishing on the reduction of the texture, the redistribution of the material and the possible reorientation of surface anisotropy. In addition, the results are compared when burnishing is performed with and without the assistance of vibrations.

Finally, it is concluded with the combination of factors that leads to better surface topography, and the following recommended steps are established for this line of research.

Acknowledgements

I would like to thank the opportunity to carry out this work, as well as all the help they have given me along the way, to my tutors J.A. Travieso Rodríguez and J. Llumà Fuentes. Also to R. Jerez Mesa, for putting up with all those questions I have asked him and for having the patience to answer them all. Thank you three for trusting me.

També vull agrair a A. Moreno per tota la força que m'ha donat per a continuar endavant durant aquest temps confinats junts. Sense tu no se on tindria el cap ara mateix.

Por último, agradecer a mis padres, a mi hermano y a toda mi familia los ánimos indispensables para concluir este trabajo. En especial a mi abuelo J.L. García, que nos estás ayudando mucho a todos. Ojalá haberte podido abrazar. Te echamos de menos.

List of symbols

Texture parameters

S parameters – surface parameters

Amplitude parameters

S_a	Arithmetical mean surface height
S_q	Surface RMS height
S_{10z}	Surface ten-point height
S_{sk}	Surface texture skewness
S_{ku}	Surface texture kurtosis

Spatial parameters

S_{al}	Fastest decay autocorrelation length

Hybrid parameters

S_{dr}	Developed interfacial area ratio
S_{dq}	RMS gradient

Miscellaneous parameters

S_{td}	Surface texture direction

V parameters – volumetric parameters

V_{mp}	Peak material volume
V_{mc}	Core material volume
V_{vc}	Core void volume
V_{vv}	Valley void volume

Abbott descriptors

S_{pk}	Abbott-Firestone peak height
S_k	Abbott-Firestone core distance
S_{vk}	Abbott-Firestone valley depth

Manufacturing parameters

a_e	Milling depth
a_p	Milling offset
b	Burnishing offset
F_p	Burnishing preload force

f_n	Milling feed velocity
h_0	Initial surface height
h_f	Final surface height
n_p	Burnishing number of passes
S^0	Original surface
St	Burnishing strategy
v_c	Milling cutting speed
v_f	Burnishing feed velocity

Abbreviations

2D	Two-dimension
3D	Three-dimension
ANOVA	Analysis of variance
DOE	Design of experiments
EDS	Electron diffraction spectrograph
FCC	Face-centred cubic
NVABB	Non-vibration assisted ball burnishing
RMS	Root mean square
TEM	Transmission electron microscopy
UTS	Ultimate Tensile Strength
VABB	Vibration-assisted ball burnishing

Index

1. Introduction

The requirements in the manufacturing industry are strictly increasing to achieve high-performance parts. The surface finish is one of the most valued aspects, not only for the aesthetic appearance of the final piece but for the great importance it has in its commissioning. It is a decisive characteristic in the resistance to wear, corrosion, and fatigue that the part may suffer, besides, to directly affecting the performance of the whole mechanism of which it takes part.

As described by Loh and Tam (1988) [1], the surface roughness is determined by all those irregularities that are characteristic of the production process that the tool leaves on the surface. There are different finishing processes with which it is intended to reduce surface roughness and achieve better finishes.

One of these processes is burnishing, which manages to correct the surface by plastic deformation. As Figure 1.1 shows, this is achieved by moving a ball or roller over the surface under a preload force. In this way, the material located in the peaks fills the valleys and thus reduces the surface roughness [2]. Despite this, some times the valleys remain intact and only the peaks are smashed, depending on the process conditions.

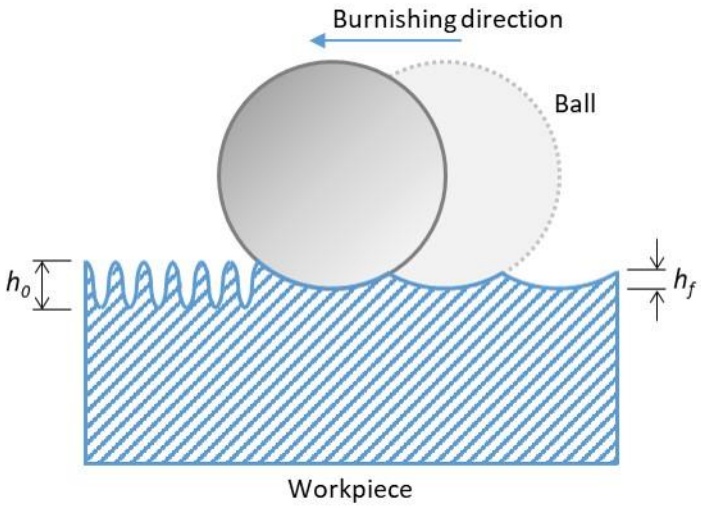

Figure 1.1. Schematic representation of the plastic deformation during the burnishing process.

Although it is still a process with a large potential for improvement, this secondary manufacturing operation has been widely investigated, as stated by Saldaña Robles et al. (2017) [3] for the state of the art of ball-burnishing. Recent research has focused on the effect that some of the process variables may have, i.e. burnishing speed, feed and force [4], friction coefficient and the tool's tip radius [5] or different lubrication/cooling strategies [6]. Furthermore, the hardening that comes with the burnishing process has also been studied [7], [8].

One of the most demanding industries in terms of quality in the manufacture of parts is aeronautics. The high safety requirements translate into rigorous quality controls, which take into account the finish and the compliance with the tolerances of all the parts. In addition, the research and development of new materials set the pace for the evolution of the sector.

In the 1940s, the first nickel-based alloys for aeronautical applications were developed. Its excellent capability to maintain high resistance at very high temperatures makes it the best material choice for turbine blades and other aerospace parts. The latest developed alloy, 720 nickel, which is evaluated and specified by the standard MSRR 7252, has the highest strength/temperature ratio and is commercially known as UDIMET®720 [9]. This nickel-base alloy is hardened both by solid solution of molybdenum and tungsten and by precipitation of aluminium and titanium. On the whole, it has not only an outstanding mechanical resistance/temperature ratio, but it also has good resistance to corrosion and oxidation [10].

To further improve the performance of 720 nickel parts, this work aims to analyse the effect of the burnishing process on the surface roughness of a milled part. To do this, 3D-roughness values have been measured. Likewise, to complete the investigation, the influence of the following variables of the burnishing process is considered: burnishing force, number of passes, feed velocity, the initial surface texture and the strategy that determines the order and direction of the passes. In the same way, it is intended to determine if there is any interaction between the burnishing force, number of passes and feed.

The process used in this work is assisted by vibrations using the vibration-assisted ball-burnishing (VABB) tool developed and characterized by Jerez-Mesa et al. (2018) [11], [12].

The effects of the VABB process were previously tested on samples of steel EN1.1176 [13] and aluminium 2017-T4 [14] by Travieso-Rodríguez et al. (2015). In both investigations, the reduction of the average surface roughness values on the samples was verified, as well as obtaining considerable improvements with a less number of passes of the tool, which allows optimizing the process times. Later, Jerez-Mesa et al. (2018) [15] adds that the steel samples obtained by the NVABB process have surface defects and scratches that can act as stress concentrators, seriously damaging the part, while the VABB samples do not have any of these defects. These improvements are related to the work-hardening that the tool generates when applying a greater plastic deformation than in the non-vibration assisted ball-burnishing (NVABB) in samples of Ti-6Al-4V [16].

On the whole, it could be concluded that the VABB process substantially improves the surface characteristics, reducing roughness and increasing the surface hardness.

To complete this study, both VABB and NVABB results are analysed to compare them and evaluate the effect of the vibration-assisted ball-burnishing process on 720 nickel alloy.

This work aims to characterize the surface texture of 720 nickel for different ball-burnishing process parameters. After an analytical and statistical study, it is intended to suggest the best burnishing conditions to enhance the surface properties. The results obtained may be of great importance for 720 nickel alloy manufacturers in order to optimize the design of the final pieces and the manufacturing processes.

1.1. Work objectives

The main objective of this work is to try to improve the surface texture of a milled 720 nickel alloy part through ball burnishing assisted by vibrations. To achieve this goal, the following sub-objectives have been established:

- Analyse the effect of 5 different factors of the burnishing process: preload force, number of passes, feed, original surface and strategy.
- Characterize the surface texture of the 720 nickel alloy using the 3D roughness parameters.
- Compare the surface affectation of the burnishing process both assisted and non-assisted by vibrations.

After the discussion of the results, it is intended to set the pace for future work by highlighting the best burnishing conditions and how to further improve the process.

1.2. Scope of work

This work is a continuation and expansion of the work done by López-Miralles (2018) [17] in his final degree project.

Before the beginning of this work, a design of experiments was chosen to optimise the experimental part. Then, the milling and burnishing operations were also carried out in the university laboratories by Jerez-Mesa [18].

Data collection has been completed with the surface and volumetric texture values obtained with an optical sensor for topographical measurements, and post-processed with the SPIP 6.6.5 software. Statistical analysis has been accomplished through Minitab 19 to determine the significant influence that the factors may have on the response parameters. Further graphs and data tables needed for the results analysis and discussion were completed with MS Excel.

2. Materials and methods

Along this section, the methodology applied in this work is explained. It starts with a brief introduction of the 720 nickel alloy and continues with the theoretical background on the 3D texture parameters to be discussed in the results, why the actual design of experiments has been chosen and all the information regarding the sample preparation and data acquisition.

2.1. 720 nickel alloy

Generally, superalloys are multiphase and multicomponent alloys that are based on nickel, cobalt, or iron. They are mainly characterized for having an outstanding long-time strength at high temperatures (> 650 °C) and high resistance to hot corrosion and erosion [19]. Among the nickel-based alloys, four different categories are found [9]:

- Disk alloys: high temperature/strength ratio requirements
- Low expansion superalloys: strict tolerance controls at high temperatures
- Superplastic alloys: capable of being superplastically formed
- Tooling low expansion alloys: for composite tooling

The 720 nickel alloy is categorized as a disk alloy, commonly known by its commercial name: UDIMET® 720. It is a trademark of Special Metals Corporation [10] and is ruled by the standard MSRR 7252. Its composition is listed in Table 2.1.

Table 2.1. 720 nickel alloy limiting chemical composition, % [10].

Ni	Cr	Co	Ti	Mo	Al	W	Zr	C	B
Balance	15.5-16.5	14.0-15.5	4.75-5.25	2.75-3.25	2.25-2.75	1.00-1.50	0.025-0.05	0.01-0.02	0.01-0.02

2.1.1. Heat treatment, microstructure and general properties

Before commissioning, a heat treatment is applied to the 720 nickel raw material. This is a standard four-step heat treatment [20], consisting of the following stages:

1) Solution treated at 1168 °C for 4 hours + air cooling at room temperature
2) Heated at 1080 °C for 4 hours + air cooling at room temperature
3) Heated at 843 °C for 24 hours + air cooling at room temperature
4) Heated at 760 °C for 16 hours + air cooling at room temperature

A schematic representation of the heat cycle is shown in Figure 2.1, along with its melting range.

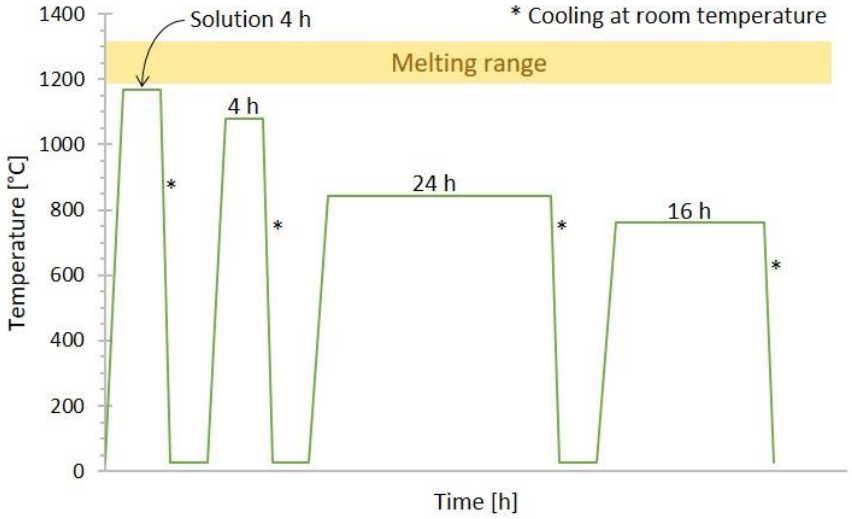

Figure 2.1. Standard four-step heat treatment cycle for 720 nickel alloy.

As a result, the basic 720 nickel microstructure is obtained. It has the following three main phases (shown in Figure 2.2): gamma matrix (γ), gamma prima precipitates (γ') and carbines and borides.

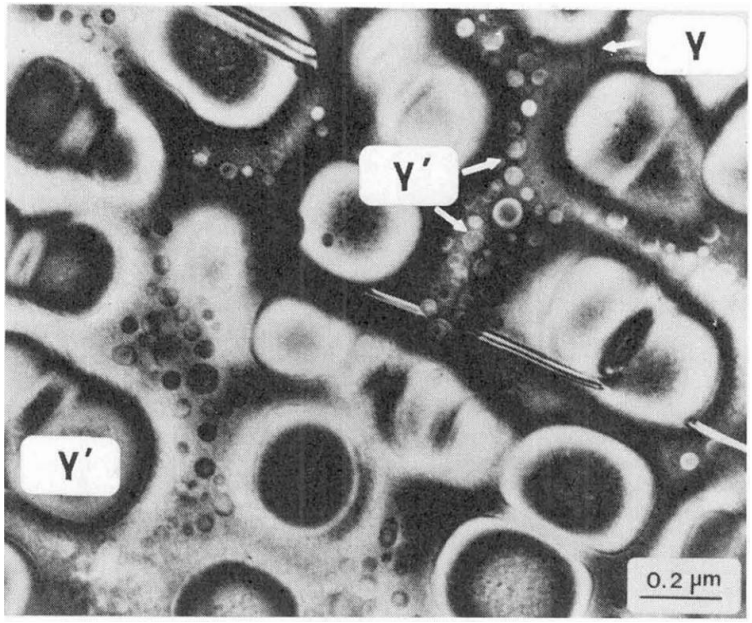

Figure 2.2. TEM micrograph of the UDIMET 720 microstructure. Phases γ and γ' are identified [20].

There is evidence of an element partition between γ and γ' phases. The matrix has a preferential presence of chromium, cobalt and molybdenum, those elements that harden the material by solid solution in a face-centred cubic (FCC) lattice of nickel. Whereas, the precipitates have a higher aluminium and titanium content, also structured in an FCC lattice $Ni_3(Al, Ti)$. The precipitates can be found in two different sizes: large precipitates (0.1 – 0.5 µm) and dispersion of fine secondary precipitates (10 – 50 nm). The interface between both phases is completely coherent [21].

The grain sizes were found to be very large, on the order of hundreds of a micron. It is a curious fact to be a material with such high mechanical properties [20].

Apart from the main phases already described, carbides and borides have also been identified throughout the microstructure. They appear with a large blocky morphology and are mostly located along the grain boundaries and twin boundaries, as shown in Figure 2.3. No significant composition difference has been found between these particles located in the grain and twin boundaries.

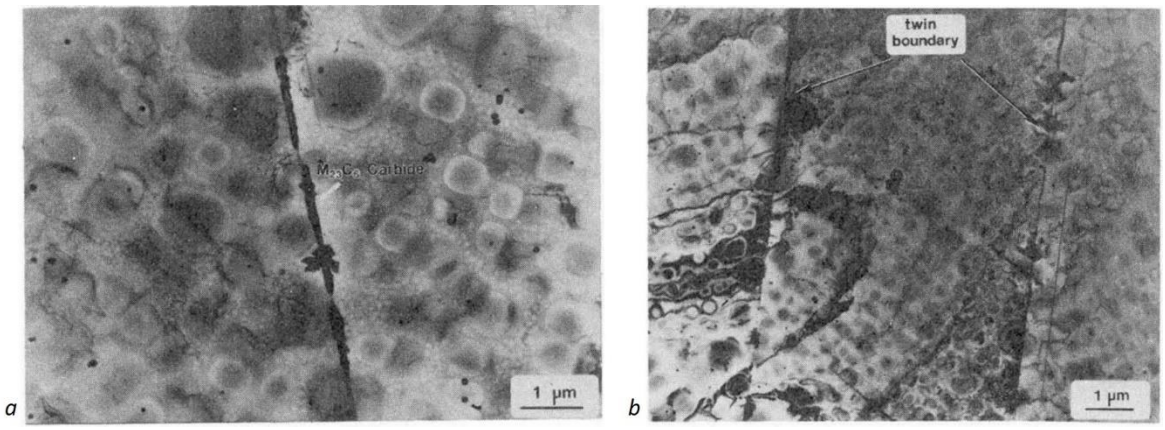

Figure 2.3. TEM micrograph of carbide particles along a) grain boundaries, and b) twin boundaries [20].

Subsequent EDS analysis has found that the carbides are mostly chromium-based, cubic structured $Cr_{23}C_6$ and also M_6C and that the borides bind primarily with molybdenum atoms in Mo_3B_2 [20]. The presence of the carbides helps to increase the high-temperature UTS [21].

Finally, the resulting properties of the 720 nickel alloy are listed in Table 2.2.

Table 2.2. 720 nickel alloy general properties [10], [22].

Property	Units	Value	
		@ room temperature	@ 875 °C
Elongation	%	4	17
Yield strength (0.2 %)	MPa	950	540
Tensile strength	MPa	1100	665
Density	g cm^{-3}	8.08	
Melting range	°C	1194-1338	
Coefficient of expansion	μm m^{-1} ºC^{-1}	12.24	

2.2. 3D texture parameters

The surface roughness has usually been characterized with the R parameters in 2 dimensions. However, the difficulty of measuring and interpreting the values is a fact, as Loh and Tam (1988) [1] pointed out since two similar values can be obtained for completely different topographies. In addition,

it must be considered that the roughness perpendicular to the burnishing process will always be greater than in a parallel profile. It is because parameters such as ball diameter or feed do not affect the latter.

That is why in this work, the 3D roughness parameters are chosen to perform the analysis. These are the so-called S –surface- and V –volumetric- parameters. According to the work of Dong et al. (1993) [23], the 3D roughness analysis and visualization techniques do not only allow obtaining a global analysis of the entire study surface but also help to understand the frequent variation of the 2D parameters.

Among the S parameters, there are four large groups according to the classification and explanation developed by Dong et al. (1994) in subsequent works [24], [25]:

- Amplitude parameters: They refer to the height distribution of the surface and have a direct correlation with the 2D parameters. The average surface texture is known as S_a, but if the root mean square (RMS) is taken, then the S_q is the response value. The difference in height between the 5 highest points (peaks) and the 5 deepest points (valleys) is represented by the S_{10z} value. The 3rd and 4th central moments correspond to the skewness and kurtosis values, respectively. S_{sk} -skewness- evaluates the asymmetry of the deviations to the mean plane of the surface, Figure 2.4. For positive values, there is a greater presence of valleys, whereas negative values show that peaks prevail along the surface. As for the S_{ku} -kurtosis-, it describes the sharpness of the measure, Figure 2.5. Values bigger than 3 are related to abrupt surfaces while smaller values represent smoother surfaces. A perfect Gaussian distribution is characterized by $S_{sk} = 0$ y $S_{ku} = 3$, with the best combination of lubricant storage, wear-off material and bearing surface, that guarantees the best functional performance of the surface.

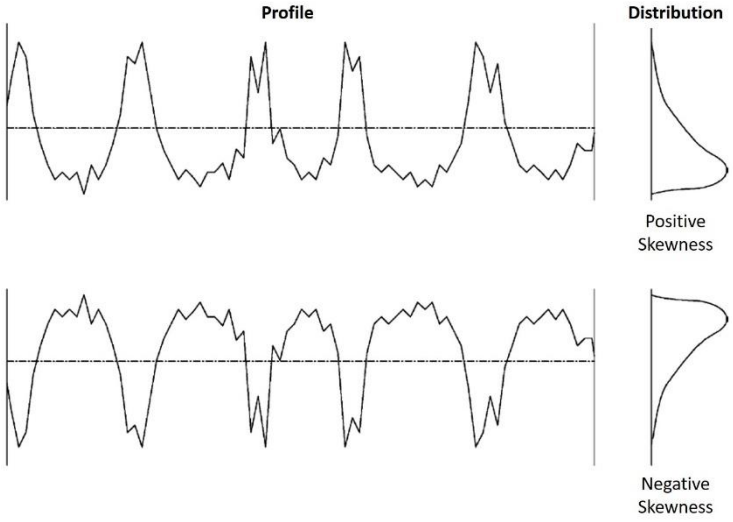

Figure 2.4. Definition of skewness parameter using a 2D profile representation [26].

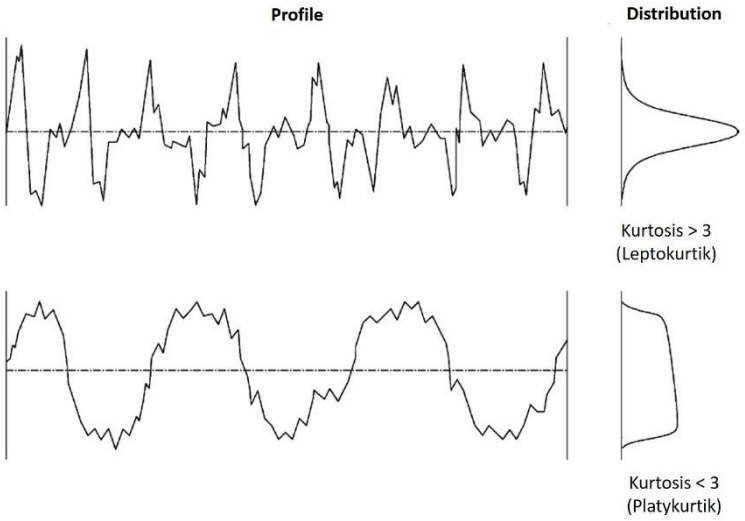

Figure 2.5. Definition of kurtosis parameter using a 2D profile representation [26].

- Spatial parameter: The S_{al} value describes the scale of the irregularities presented by the surface. The higher the value, the lower the repetition frequency and the greater the dimension of the irregularity.

- Hybrid parameters: They are a mix of amplitude and spatial parameters. The S_{dr} value is a ratio of the actual interface area to its flat projection. High values adjust to very rough surfaces, while values close to zero present a surface near from finishing. Surfaces with $S_{dr} \leq 1\%$ are considered to correspond to already finished surface topologies. The calculation in RMS is known as S_{dq}.

- Miscellaneous parameter: This parameter is the angle of the main direction of the texture pattern, and is known as S_{td}.

The S parameters calculations in this work follow the ISO 25178 standard. Annexe A shows all the equations corresponding to the above-mentioned parameters.

V parameters refer to the volumetric distribution of the material and voids along with the height of the surface topology. This method differentiates three areas: peak, core and valley. The material volume corresponding to the peak (V_{mp}) represents the material that wears off more easily. The core is a balance between material (V_{mc}) and void (V_{vc}) that determines the bearing capacity of the surface. And finally, the valley refers to that void volume (V_{vv}) that keeps lubricant and evacuates debris. This classification follows the ISO 13565-2 standard and states that the first 10% of the accumulated height corresponds to the peak and the last 20% belongs to the valley.

The mentioned volumetric parameters are an alternative to the traditional bearing curve developed by Abbott [27]. In this case, a parallel line to the point with the lowest slope is drawn, and the intersections with the Y-axis at 0 and 100% of the accumulated height determine the rank of height

corresponding to each area. The parameters that characterize the curve are S_{pk} (peak height), S_k (core height), and S_{vk} (valley height).

2.3. Design of Experiments

The design of experiments (DOE) are classic statistical models that help to assess whether the study factors influence the analysed response and to quantify this influence.

The burnishing process depends on different variables. In this work, five factors are evaluated at three levels to test the effects on topological parameters of the VABB burnishing process in a 720 nickel alloy part. Table 2.3 includes the values assigned to each factor, which can be defined as:

1. Preload force, F_p: this is the static compression force exerted by the tool to the surface. The target value is established before the burnishing begins at the starting point and it is not readjusted during the process.
2. Number of passes, n_p: is the number of times that the burnishing is performed on the same study area. A larger number of passes is expected to apply higher plastic deformation.
3. Feed, v_f: the linear speed at which the tool moves through the surface.
4. Original surface topology, S^0: the surface finish of the initial surface obtained by different milling parameters. The milling conditions are further described in section 2.5.
5. Strategy, *St*: is the path followed by the tool to cover the whole study area. Figure 2.6 shows a schematic representation of the three strategies combined with the number of passes.

Table 2.3. Factors and levels considered in the design of the experiment.

Factor	Level		
	1	2	3
F_p [N]	150	300	450
n_p	1	3	5
V_f [mm/min]	300	600	900
S^0	1	2	3
St	nb0	bn90/0	bn0

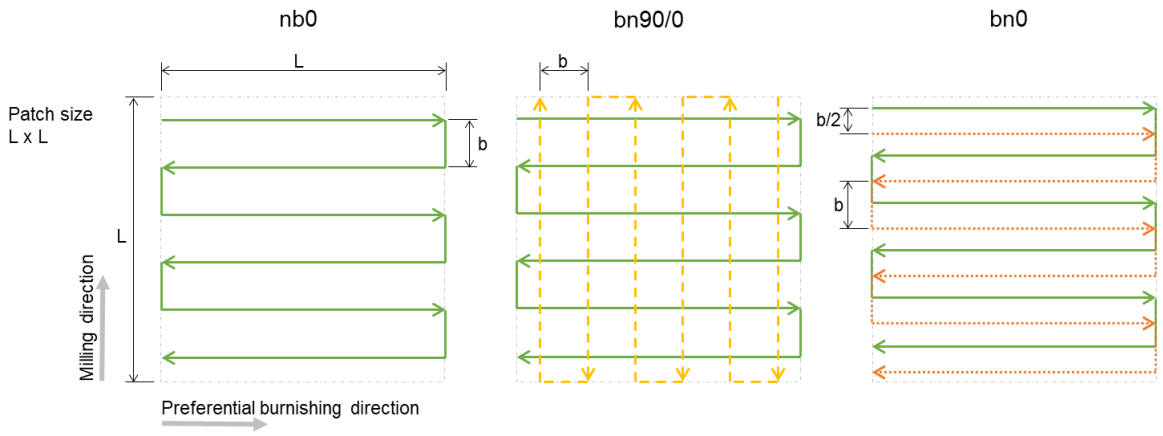

Number of passes	Strategy		
	nb0	bn90/0	bn0
1	→	→	→
3	→ → →	→ -> →	→ ⇢ →
5	→ → → → →	→ -> → -> →	→ ⇢ → ⇢ →

Figure 2.6. Schematic representation of the three different strategies for each level of the number of passes.

Using the traditional factorial design to plan the experiments would involve 3^5 = 243 experiments to evaluate the five factors at all three levels. This is a large number of tests, which implies a higher material expense, time and other resources.

In order to reduce them, the method described by Taguchi (2005) [28] is applied, which minimizes the number of experiments although the study of all five factors is maintained as a first-order effect. Among the available orthogonal matrices, the one that best adapts to the current work is L27, as previously found Jerez-Mesa [18]. It is capable of evaluating up to 13 factors at 3 levels, with only 27 experiments (see Annexe B).

Besides the possibility of evaluating the direct influence of each factor, L27 still has degrees of freedom, as shown in Figure 2.7. That allows assessing whether up to three pairs of factors may be related to each other to analyse their interaction.

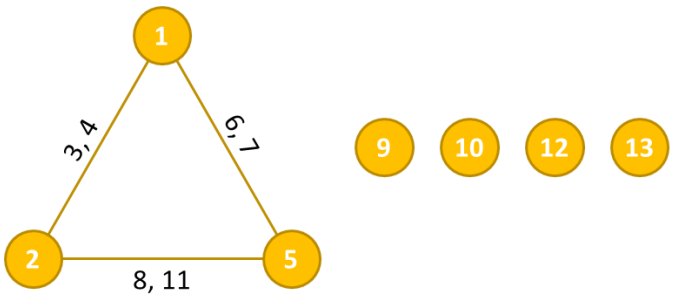

Figure 2.7. Linear graph representing the interactions between the 13 different columns in L27 orthogonal array.

The DOE is completed by assigning a column to each factor. Taking advantage of the second-order influence between columns 1, 2 and 5, they are assigned to preload, number of passes and feed velocity, respectively. These three factors set the parameters of the burnishing process itself. No interactions involving the initial surface (column 10) and strategy (column12) are expected.

Finally, the definite matrix is shown in Table 2.4, with the burnishing conditions corresponding to each run or experiment according to the level of each factor.

Table 2.4. Burnishing conditions according to the L27 matrix called for the design of the experiment.

Run	Fp [N]	np	Vf [mm/min]	S0	St
1	150	1	300	1	nb0
2	150	1	600	2	bn90/0
3	150	1	900	3	bn0
4	150	3	300	2	bn0
5	150	3	600	3	nb0
6	150	3	900	1	bn90/0
7	150	5	300	3	bn90/0
8	150	5	600	1	bn0
9	150	5	900	2	nb0
10	300	1	300	3	bn90/0
11	300	1	600	1	bn0
12	300	1	900	2	nb0
13	300	3	300	1	nb0
14	300	3	600	2	bn90/0
15	300	3	900	3	bn0
16	300	5	300	2	bn0
17	300	5	600	3	nb0
18	300	5	900	1	bn90/0
19	450	1	300	2	bn0
20	450	1	600	3	nb0
21	450	1	900	1	bn90/0
22	450	3	300	3	bn90/0
23	450	3	600	1	bn0
24	450	3	900	2	nb0
25	450	5	300	1	nb0
26	450	5	600	2	bn90/0
27	450	5	900	3	bn0

It should be noted that the fact of being burnished with or without vibrations is not considered as a factor in the DOE, but two L27 matrices are actually carried out. Consequently, 54 experiments are performed, distributed in the study surfaces as explained in section 2.5.

2.4. Analysis of Variance

An ANOVA (Analysis of Variance) is a statistical analysis that allows determining whether there is a significant difference between the means of different populations using the hypothesis test, one of the most used methods in decision-making based on sample statistics. To check the factors that show statistical significance on the response, the p-value is analysed. The p-value is the probability that shows the evidence against the null hypothesis (H_0). For smaller p-values, there is stronger evidence that the null hypothesis is not true.

In this case, the null hypothesis states that there is no influence between factor and response. So, if a factor does influence any of the selected parameters as a response, the H_0 should be rejected.

The way a p-value is evaluated to confirm whether the H_0 is accepted or rejected is by comparing it with the significance level (α). The significance level is the maximum established risk of concluding that the H_0 is not accepted when it should be. α=0.100 is established in this study, that means that at least a 10% probability of the wrong conclusion is accepted. Then, these two cases are possible:

- p-value ≤ α: the H_0 hypothesis is rejected and that factor has a statistical influence on the response.
- p-value > α: the H_0 cannot be rejected and the influence is not statistically significant.

The ANOVA results can be also graphically represented in the main effects plot, which shows the mean value of the response parameter for each factor level. The main effect exists when different levels of a factor affect the response differently. This affectation can be evaluated with a visual analysis of the slope of the line connecting the points of a factor:

- Horizontal line: all levels affect the response in the same way, this is that the factor has no mean effect.
- Non-horizontal line: levels affect the response differently, so there is a main effect. The higher the slope, the greater the affectation of the main effect.

2.5. Sample preparation & VABB tool

The raw material used is a 117 mm diameter cylindrical block of 720 nickel alloy obtained by forging. On one of the circular bases of the block, three different surfaces have been machined: the initial surfaces, S^0. The milling process is carried out with a 10 mm diameter hemispherical milling following the parameters set in Table 2.5.

Table 2.5. Milling parameters for the three initial surfaces.

Original surface	Machining parameters				
	a_e [mm]	a_p [mm]	v_c [m/min]	f_n [mm/rev]	Tool Ø [mm]
S^0_1	0.5				
S^0_2	0.7	0.2	60	0.1	10
S^0_3	1.1				

These milling parameters are schematically represented in Figure 2.8.

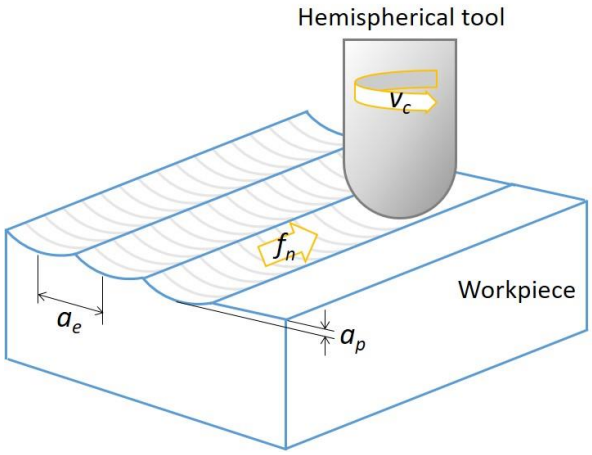

Figure 2.8. Schematic representation of the milling parameters.

Once the three milling surfaces are done (three different big coloured areas in Figure 2.9), the 54 burnishing runs are performed with an offset b = 0.3 mm (Figure 2.6) following the conditions previously set by the DOE in Table 2.4. The vibration frequency of the tool for the VABB runs were executed at 40 kHz. Each run was performed in a 10 x 10 mm footprint.

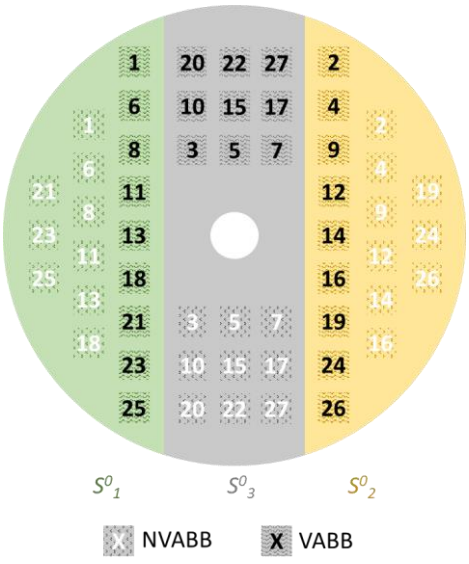

Figure 2.9. Overview of the location distribution of the 54 runs performed in the 720 nickel alloy sample.

To perform the VABB operations, the tool presented in Figure 2.10 is used. As detailed by Jerez-Mesa et al. (2018) [11], the tool is made up of three different modules. Inside the tool holder, there is a spring that, when compressed with a certain preload, burnishing force is exerted on the surface of the material. The intermediate module contains four piezoelectric disks, which generate a vibration in phase with the alternate voltage that polarizes them. The last module supports the burnishing ball and allows both preload force and vibration to be transmitted to the workpiece.

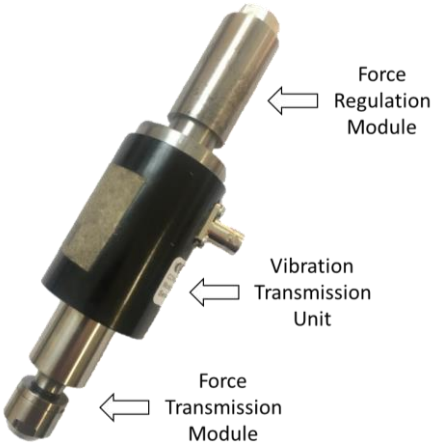

Figure 2.10. Vibration-assisted ball burnishing tool and its modules.

With this tool, it is also possible to work without vibration when the piezoelectric disks are not excited. The maximum preload that can be applied is 500 N with the current tool.

2.6. Data acquisition

All roughness parameters previously explained have been acquired by a CCS Prima Optical Pen CL1-MG210 sensor for topographical measurements. It was mounted in the 3D micromeasure station from STIL: Stand Micromesure 2 (Figure 2.11), and controlled through the data acquisition software Surface Map. Before taking measurements, the footprint surface has been cleaned with pure ethanol.

Figure 2.11. Stand MIcromesure 2 from STIL with an optical sensor [29].

For each sample, a 3D mapping of a minimum 1:1 ratio surface area has been performed to ensure 6 pairs of peaks and valleys of the footprint (see subsection 2.6.1). The distance between measurements in the square patch is between 15-20 µm in both directions.

The post-processing of the data has been done through SPIP 6.6.5 software. After an almost mandatory need to level the sample, it takes de 3D map, calculates all the required parameters, allows to graph the results and perform different kinds of analysis. Besides, the correction that some runs may need is also performed in SPIP. Subsection 2.6.2 further explains the error corrections that have been carried out. A template has been designed to collect all the data obtained from each run (see Annexe C).

2.6.1. Patch size

Due to the time required to acquire 3D roughness data, the studied area has been minimized according to a preliminary study carried out by Jerez-Mesa et al. (2018) [15]. It looks for the minimum amount of peak-valley pairs necessary to obtain representative values of that surface. In order to find the most optimized patch size, the most relevant responses are plotted as the number of peak-valley pairs increase.

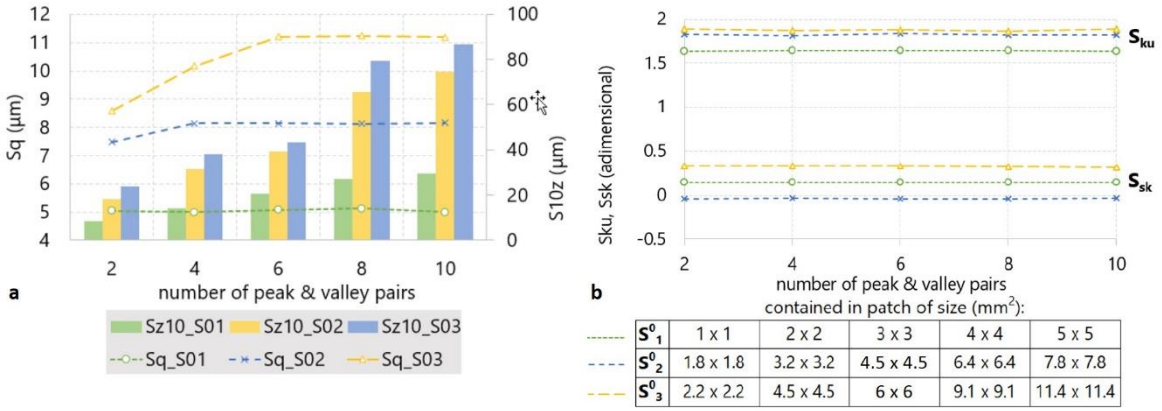

Figure 2.12. Evolution of the S_q, S_{10z}, S_{sk}, and S_{ku} with the number of peak-valley pairs [18].

Finally, the results convergence stabilizes from 6 peaks and valleys of the original surface, which determines the minimum area necessary to make the measurements. In this way, the dimensions of the footprints of each of the surfaces are obtained and presented in Table 2.6.

Table 2.6. The minimum area that ensures measurements of 6 peaks and valleys for each original surface.

Initial surface	Patch size [mm^2]
S^0_1	3 x 3
S^0_2	4.5 x 4.5
S^0_3	6 x 6

2.6.2. Error correction

During the visualization of the 3D roughness data, two types of errors were detected in various footprints:

- Outliers: extremely high or low isolated points due to surface debris
- White voids: non-measured points due to very high surface inclinations, from which the sensor could not receive a signal

Different solutions have been applied depending on the type of error:

- Very high and coarse isolated peak: the surface is cleaned again and a new measurement is performed
- Low and fine isolated peak: correction by software through the "Remove Outliers" tool (see Annex D1)
- White dots: correction by software through the "Void Pixels" filling tool (see Annex D2)

The variation in the results of the corrected samples before and after the correction has been around ± 5 %. This is a very small variation, and all corrections by software are considered valid.

3. Results and discussion

Throughout this section, the results obtained are shown and discussed following a logical order in the presentation of the results. First, a preliminary analysis of the three original surfaces is carried out. Then, the S parameters' results obtained for the VABB process are extensively discussed. The V parameters are also analysed with a consideration on its usefulness. And finally, a comparison between the VABB and NVABB processes is presented.

3.1. Original surfaces

As explained previously in section 2.5, the only difference between the original surfaces is the offset, a_e, during the last milling pass. In this result's subsection, the difference in texture parameters between the three S^0 is analysed. Figure 3.1 collects the texture S values obtained for each initial surface.

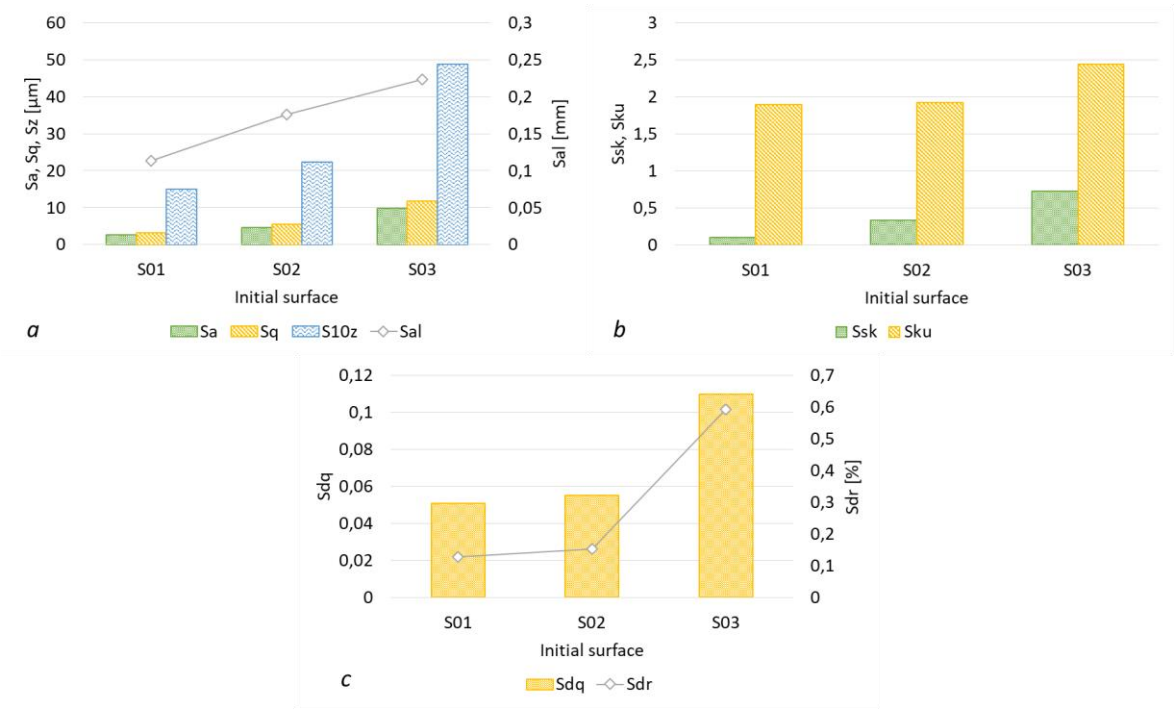

Figure 3.1. 3D surface texture parameters of the original surfaces: a) amplitude and spatial parameters, b) skewness and kurtosis, and c) hybrid parameters.

In all three cases, the S_a and S_q values are adjusted to the relationship established by King and Spedding (1982) [30] with the skewness and kurtosis values: in this case between 0.84-0.86 (Annexe E). The analysis of both values becomes redundant and, therefore, it is possible to ignore the results of S_a due to its lack of statistical essence.

In general terms, it can be seen how all the plotted parameters grow from S^0_1 to S^0_3. For S_q, this increment is consistent with the milling offset increase: larger offsets lead to a bigger sample standard deviation in height.

Regarding kurtosis, the three original surfaces are platykurtik with an increasing trend: S^0_3 is the surface with S_{ku} closer to 3. For skewness, S^0_1 shows the closest value to 0 and there is also an increasing trend through positive values: as the offset in the milling process grows, the material shifts to the peaks. Thus, none of the original surfaces is more quasi-Gaussian than the others.

The progressive growth of S_{al} indicates that the repetition frequency is getting smaller, that is, the surface irregularities are on a larger scale. This is predictable, as it is consistent with the increasing offset separation in the original milling parameters, a_e. Besides, it presents a greater difference in height between the deepest valleys and the highest peaks, S_{10z}. This upward trend confirms that S^0_3 is the most abrupt starting surface, while S^0_1 is the smoother. However, considering the hybrid parameters, the three surfaces correspond to already finished surfaces: all three S_{dr} values are well below 1%. Only the S_{dr} parameter will be considered in the discussion of the hybrid parameters because both values refer to the same surface characteristic but the S_{dq} is not so intuitive.

Considering the volumetric parameters, they also show an increasing trend in Figure 3.2.a: the amount of material and void for the peak, core and valley are maximum for S^0_3. However, whereas for S^0_1 and S^0_2 there is around two times the volume corresponding to void valleys (V_{vv}) than material peaks (V_{mp}), for S^0_3 this relation flips over and shows that the peaks have a slightly predominant presence over the valleys.

This particular surface distribution presented by S^0_3 is contrary to the previous skewness statement. The greater the S_{sk} within the positive range, the greater the presence of valleys.

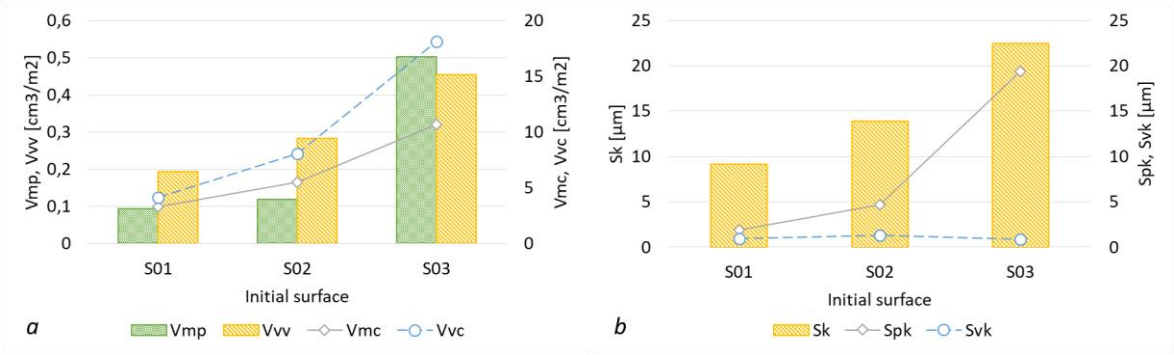

Figure 3.2. 3D texture parameters of the original surfaces: a) volumetric parameters, and b) Abbott curve parameters.

The general increasing trend is also respected by the Abbott curve descriptors (Figure 3.2.b), except for the height of the valley, S_{vk}, where the maximum value is presented in case of S^0_2, although all three

surfaces show very close values. In the same way as the volumetric parameters of S^0_3, all S_{pk} values are higher than S_{vk}, completely disagreeing with the skewness statement.

3.2. VABB results

This subsection collects the results regarding the S parameters for the VABB process. The results have been structured following the triple topological effect found by Jerez-Mesa et al. (2018) [15] when analysing the surface texture after VABB burnishing on AISI 1038 alloy: surface reduction, height redistribution and anisotropy reorientation of the surface.

3.2.1. Surface texture reduction

In order to analyse the influence of the VABB factors in the surface texture height, the response parameters S_q, S_{10z}, and S_{dr} are called. As described previously by Jerez-Mesa et al. (2018) [15], the analysis of these 3 parameters is enough to define the surface height reduction. An ANOVA has been conducted to analyse the statistical influence of all described factors.

Table 3.1 collects all the p-values obtained for the five factors and the three pairs of interactions. The shaded values correspond to those p-values that are below the significance level.

Table 3.1. VABB p-values obtained for Means. Shaded values are below α=0.1.

Response	Analysis of Variance for Means							
	F_p	n_p	v_f	S^0	St	F_p*n_p	F_p*v_f	n_p*v_f
S_q	0,024	0,045	0,967	0	0,832	0,807	0,778	0,840
S_{10z}	0,084	0,028	0,895	0	0,554	0,758	0,469	0,786
S_{dr}	0,081	0,069	0,607	0,001	0,212	0,125	0,144	0,421

It is seen the great influence exerted by the initial surface topology with an absolute 0 as p-value. That means that, with the analysed data, there is a 0% probability of the wrong conclusion that the S^0 has an influential effect on the response parameters. The preload and number of passes for S_q, S_{10z} and S_{dr} also show mean p-values below α. However, the p-values obtained for the speed and strategy are much higher than the significance level, that is that factors v_f and St do not influence any of the responses.

In addition to the self-influence of each factor, it is intended to determine if a relationship exists between those three factors that set the burnishing process -preload, number of passes and feed velocity-. The three possible pairs have been added to the ANOVA and the mean p-values for all cases are well over α. Indeed, there is no interaction between factors.

To sum up, the original surface is proved to be the only common influential factor and that there is no interaction between factors for any of the responses. To complete this statement, as S_q is considered the most significant value to characterize the whole surface texture, its potential for improvement is also analysed. Especially to check how the initial surface influences the final texture after burnishing.

The improvement ratio $1 - {S_q}/{S_q^0}$ is considered and subjected to an ANOVA, Figure 3.3. It is seen how surface S^0_1 has a notable much higher potential of improvement than S^0_2 and S^0_3. It can be said that the finer the original surface, the greater the improvement of the surface texture thanks to the burnishing process.

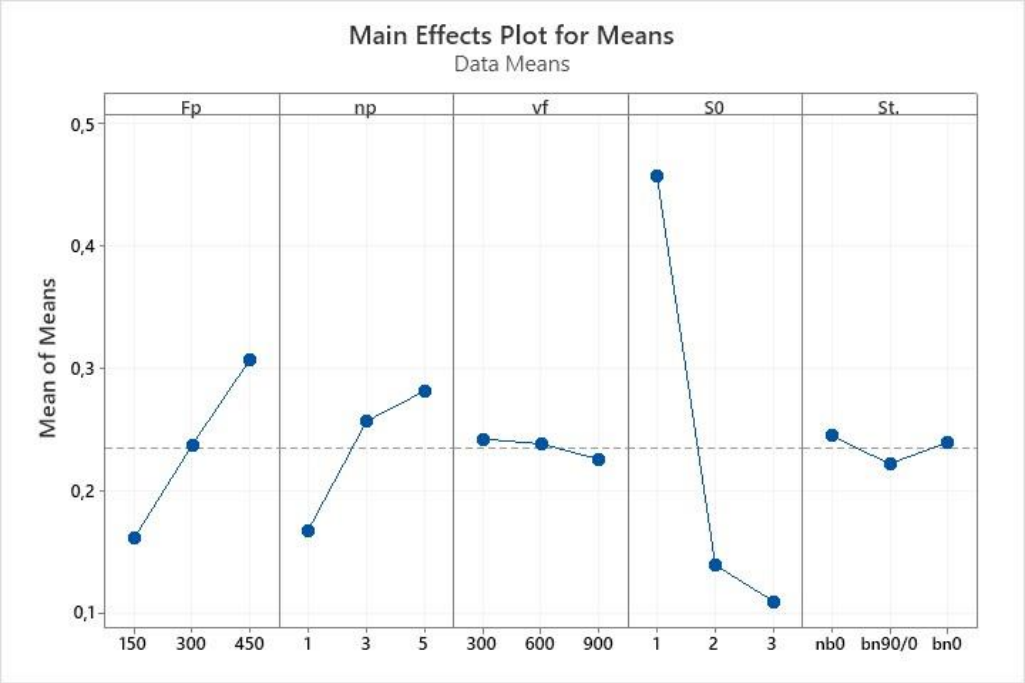

Figure 3.3. Main effects plot for means of the S_q potential of improvement: 1-S_q/S_q^0 for the VABB runs.

Now that it is known whether the factors influence or not and how much, it is analysed how they influence. Figure 3.4 shows the evolution of the previously mentioned amplitude and spatial parameters as the plastic deformation is increased (number of passes and preload force) for the VABB runs. Considering that the original surface is the most influential factor, the runs have been ordered according to S^0 to facilitate the reading of the results.

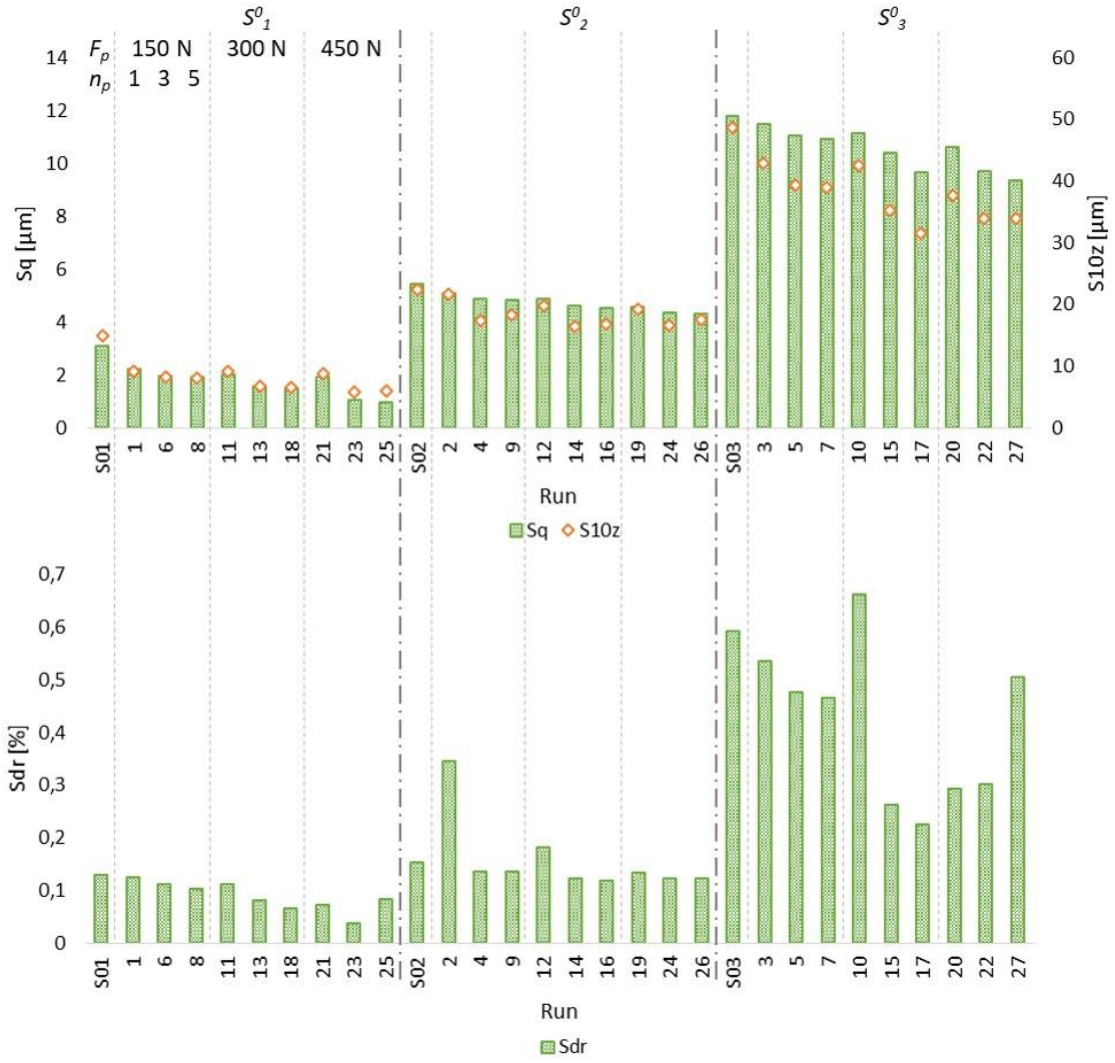

Figure 3.4. S amplitude and hybrid parameters that characterize the VABB runs.

For the three surfaces, it can be seen how the S_q value gradually decreases as the plastic deformation increases (higher preload and number of passes). Despite that, in the same way as the results obtained by Jerez-Mesa et al. (2018) [15], when the preload increases and the number of passes turns back to 1 –i.e., from 150 N & 5 p to 300 N & 1 p and from 300 N & 5 p to 450 N & 1 p-, the S_q increases as well. It is because even the preload is higher, just one pass is not enough to increase the net plastic deformation compared to the previous run –with lower preload but 5 passes-. But in a general overview of the results, there is a clear S_q reduction related to the plastic deformation increase. On the contrary, the same author found that for the smoother initial surface there was a threshold of plastic strain that leads to surface harm by increasing S_q. In this analysis, this limit does not appear, and this could mean that the 720 nickel surface roughness can still be improved by applying more plastic strain. However, further analysis should be done to avoid being in the limit of surface damage since it could lead to embrittlement and a reduction of the in-service conditions.

As mentioned above, the number of passes has been confirmed to be one of the influential factors for the S_q results. Despite this, Figure 3.4 does show a significant difference between the values corresponding to 1 and 3 passes, whereas those for 3 and 5 passes seem to be extremely close. Applying the same preload as the very first pass during the whole process may be the cause. The affectation in previous passes has already sufficiently modified the surface so that the fifth pass does not show a great evolution. This effect is shown in Figure 3.5.

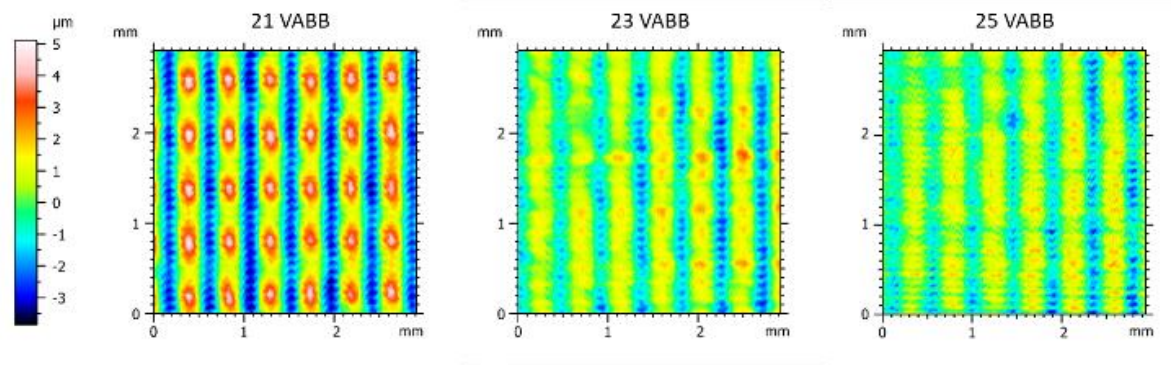

Figure 3.5. Pseudo-colour view of S^0_1 surfaces VABB burnished with 450 N and 1 pass (#21), 3 passes (#23), and 5 passes (#25) with the same height-scale for visual analysis of the affectation of the number of passes.

Similarly, S_{10z} decreases significantly from 1 to 3 passes, but not from 3 to 5 passes: the values are extremely close and no tendency is observed. However, in S^0_2 a slight increase is appreciated from 3 to 5 for all three preloads. As this effect is only seen in the intermediate surface and there is no statistical explanation for this behaviour, no certainty can be deduced.

As expected, the S_{dr} ratio decreases with the plastic deformation, so there is less interfacial surface area relative to the projected area, which means that with surface reduction, a more super finished surface is achieved. It is also seen that some values deviate from the general trend; this may be due to the high sensibility of this response parameter.

3.2.2. Height distribution

The surface parameters that allow a height distribution analysis are skewness and kurtosis values. As previously explained in section 2.2, the best-balanced surface in terms of material and void distribution is that with a Gaussian distribution, with skewness and kurtosis equal to 0 and 3, respectively. Figure 3.6 shows the evolution of both parameters of VABB runs as more plastic deformation is applied. It can be found that the three surfaces perform differently.

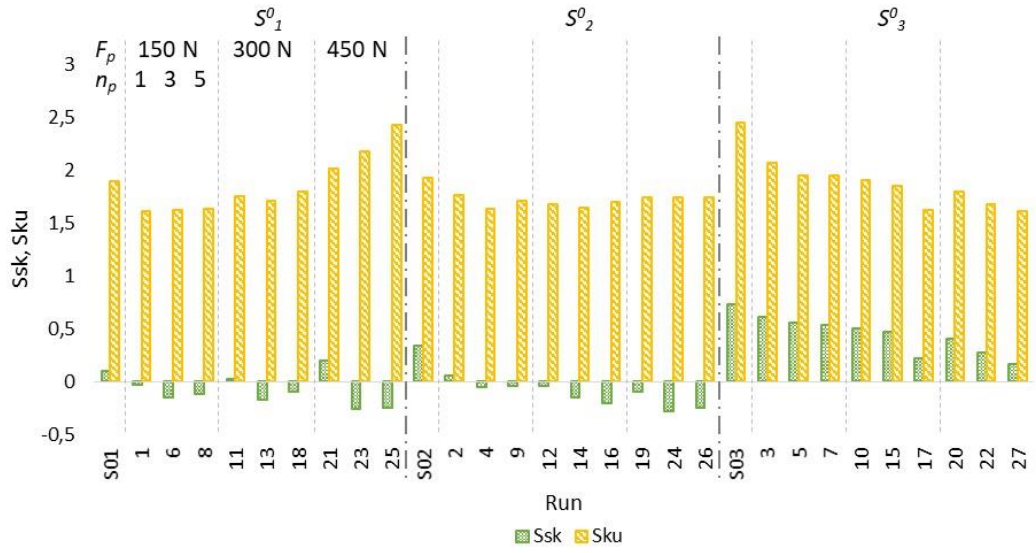

Figure 3.6. Skewness and kurtosis parameters for VABB.

Taking a look at the evolution of the runs performed on S^0_3, the skewness is always found to be above zero with a decreasing trend as the plastic deformation increases, i.e. the last run, #27 is almost 0. This agrees with the evolution of the histograms corresponding to S^0_3 runs (Figure 3.7), which shows a bigger accumulated height for valleys on the original surface, and how it is stabilized until an almost equilibrium between the area above and under the 0 line, in the last run #27. On the contrary, kurtosis shows singular behaviour. As the texture, S_q, is reduced, the S_{ku} values recede from value 3 and, therefore, from a Gaussian distribution. This evolution enhances bimodality. As plastic strain is applied, it is possible to reduce significantly the roughness, but towards an unsuitable distribution. However, it should be tested in further investigations whether applying even higher plastic deformation, the kurtosis gets closer to values 3 again. Jerez-Mesa (2018) [18] found that the bimodality is the previous step to monomodal.

For S^0_2 runs, there is no clear trend in the Kurtosis values besides being very close. Consequently, even the roughness decreases -the histogram narrows in Figure 3.7-, the trimodality is maintained. Additionally, in this case, the S_{sk} gets smaller and smaller below zero. That means that the new material distribution is increasingly concentrated in the upper zone.

Finally, a completely different situation is observed in S^0_1. Even there is no trend in the skewness evolution, all values are very close to 0. That leads to well-balanced distributions of material on both sides of the average plane, as shown in the histograms for surface S^0_1. Checking the S_{ku} values, a first decrease for the 150N preload is observed, but for 300N it rises again. For 450N the increasing trend is maintained and reaches the maximum value for 5 passes of all VABB runs. These limit conditions – smoother initial surface, higher preload and the maximum number of passes- have led to the

narrowest and only unimodal distribution obtained. Run #25 can be considered as a quasi-Gaussian distribution with the best balance between wear material, lubricant retention, and bearing surface.

On the whole, the only common fact for all the runs and initial surfaces is that all of them are platykurtik, $S_{ku} < 3$. Besides, in all cases, the height distribution narrows with plastic strain.

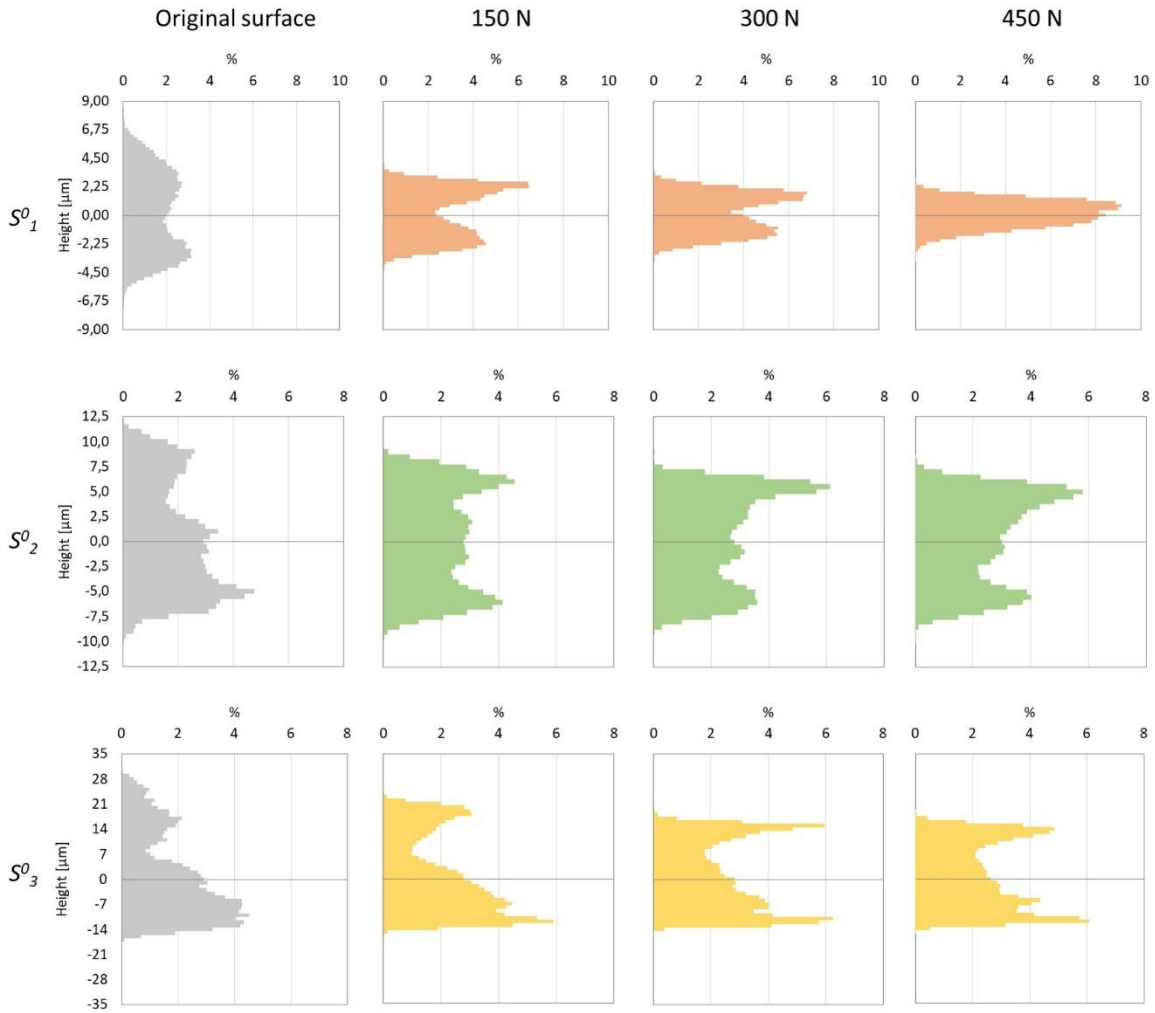

Figure 3.7. Height histograms evolution with the preload (from left to right: original, 150 N, 300 N, and 450 N) and initial surface (from top to bottom: S^0_1, S^0_2, and S^0_3) for the VABB process for the same number of passes, 5.

3.2.3. Anisotropy reorientation

The third expected effect of the burnishing process is the reorientation of the surface texture. As previously seen in Figure 2.6, the preferential direction of the burnishing process is perpendicular to the milling direction. This fact may lead to surface reorientation if the plastic deformation applied is enough. The most suitable parameters to analyse this effect are the spatial and miscellaneous parameter.

S_{al} shows in Figure 3.8 the same trend for S^0_1 and S^0_2 runs: when applying plastic strain, the value decreases from the original surface and remains constant regardless of preload and number of passes. That is, the repetition frequency of the irregularities increases under permanent deformation but no matter how much is applied. Despite this, for S^0_3 there is no variation from the original surface, so the scale of the irregularities is not modified.

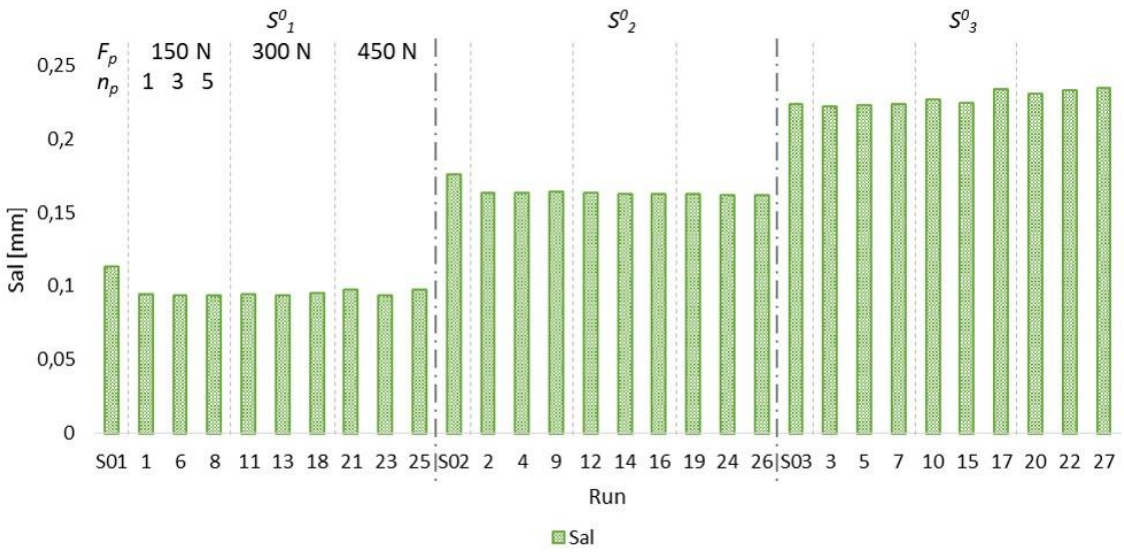

Figure 3.8. Sal values for the VABB runs.

Considering the preferential texture direction, the three original surfaces S^0 are oriented at 90° respect to the X-axis. After burnishing, no changes in the 1st preferential direction are observed in Figure 3.9. That is, the original milling pattern can still be seen after any burnishing conditions tested in this study. The affectation is not enough to reorientate the primary surface texture. However, the 2nd and 3rd directions fluctuate between different values. At first, it could be associated to the evolution of the plastic strain (a combination of preload and number of passes), but also with the strategy factor, which in some cases adds burnishing passes in the milling direction.

The first hypothesis can be qualitatively discussed in Figure 3.9, where no common trend is appreciated for the three S^0. $S_0{}^3$ presents an outstanding preference direction at 45 ° with a few fluctuations. On the contrary, S^0_2 has an exaggerated and senseless fluctuation. And finally, even S^0_1 also shows a little fluctuation, in this case, a trend in 2nd direction can be appreciated: for preloads 150 and 300 N, the angle is kept around 20 °, but from the first run with 450 N, the angle drops to 0 for all numbers of passes. This is, that for the smoother surface, the higher preload applied is capable of modifying the surface texture sufficiently to add the burnishing preferential direction. Instead, the burnishing has not applied enough plastic deformation to affect the most abrupt surface.

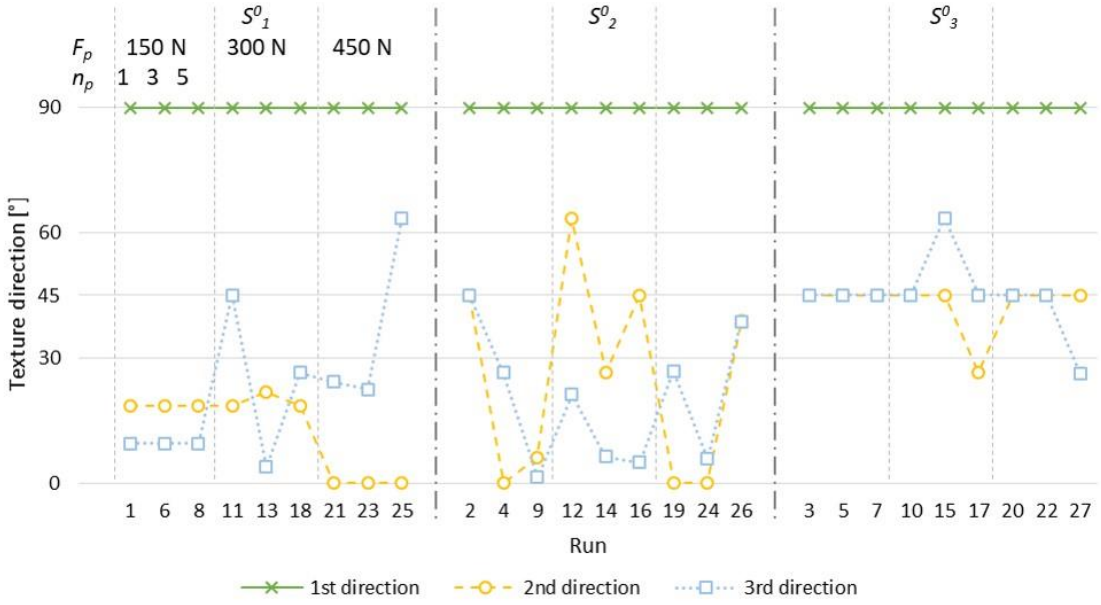

Figure 3.9. 1st, 2nd and 3rd preferential texture directions for VABB runs.

This fact is also enhanced taking into account the frequency of the spectrum (quantitative analysis). For example, even runs 4, 19 and 21 VABB show the same the three preferential directions (1st direction: 90 °, 2nd direction: 0 °, and 3rd direction: approximately 26 °), their spectrums are completely different, Figure 3.10. It shows how, even for the three runs there is a 2nd preference direction at 0 °, the frequency is much higher as the plastic strain increases with a higher impact on the smoother surface, run 21 VABB. This is why the tendency shown by the 2nd direction in S^0_1 (Figure 3.9) is so relevant: the frequency at 0 ° also turns higher throughout runs 21, 23, and 25, so the plastic strain enhances the direction changes in the surface texture.

For the second hypothesis referring to the possibility that the strategy factor, *St*, has something to do, an ANOVA has been conducted for the 2nd and 3rd directions. The 1st direction has been ignored because it is always 90 °. The results obtained are shown in Table 3.2 with a significance level of 10%, which denies that there is any relationship between the angles and the strategy. Again, the only influential factor is the original surface, and there is no interaction between factors.

Table 3.2. VABB p-values for the 2nd and 3rd texture directions. Shaded values are below α=0.1.

Resp.	Analysis of Variance for Means							
	F_p	n_p	v_f	S^0	*St*	F_p*n_p	F_p*v_f	n_p*v_f
2nd	0,396	0,687	0,892	0,082	0,742	0,804	0,627	0,886
3rd	0,769	0,662	0,663	0,098	0,862	0,734	0,475	0,721

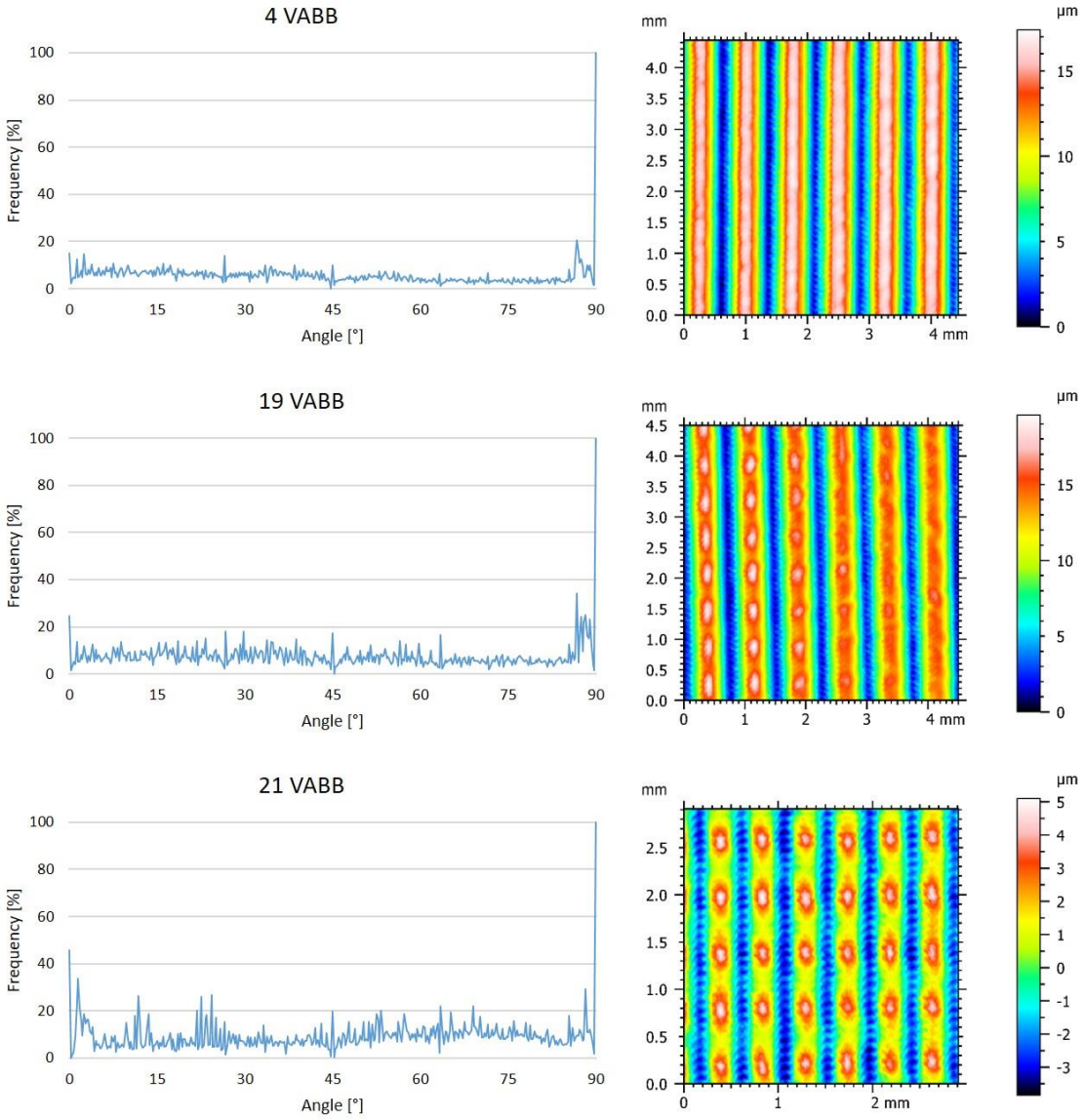

Figure 3.10. Comparison of the frequency spectrum and the pseudo-colour view for runs 4 VABB, 19 VABB and 21 VABB, which present the same three preferential texture directions: (1st direction: 90 °, 2nd direction: 0 °, and 3rd direction: approximately 26 °).

3.3. Volumetric parameters and Abbott curve

Comparing the volumetric parameters with the descriptors of the Abbott curve, several differences are found. Both sets of parameters are plotted in Figure 3.11. There are also differences with the previous discussion resulting from the S parameters.

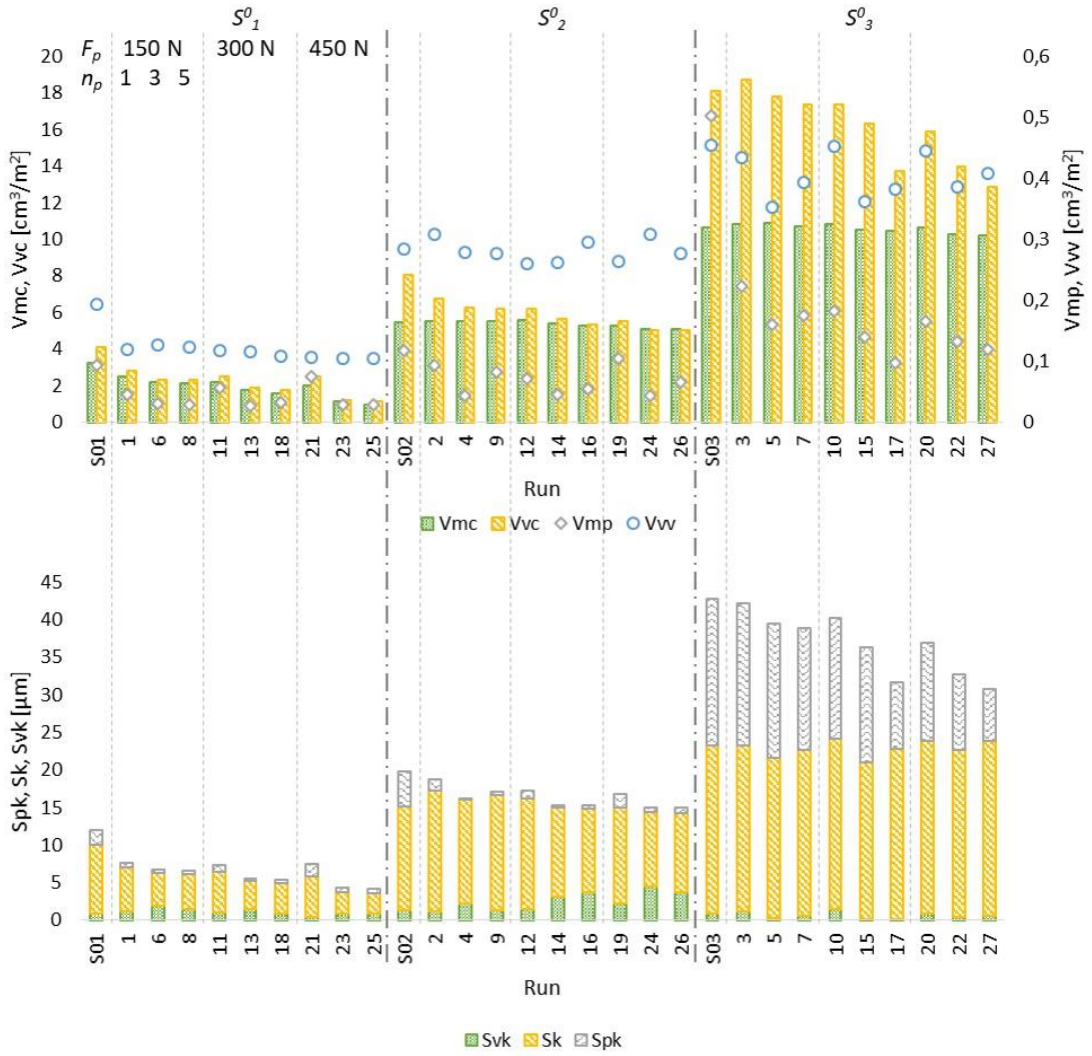

Figure 3.11. Volumetric parameters and Abbott descriptors for VABB runs.

As expected with the Sq decrease, and although there are some exceptions, the material located in the core zones (S_k and V_{mc}) shows the same downward trend concerning the initial surface. However, V_{mp} and V_{vv} are widely dispersed and show no clear evolution. Both parameters were also expected to decrease as the plastic strain smashes the peak material. In any case, all runs except the original S^0_3 have volumetric parameters V_{vv} values much higher than V_{mp}, but not for the Abbott criterion. For S^0_1 and S^0_2, the relationship of the curve descriptors for the peak and valley is quite random, but for S^0_3 it's completely the opposite: the values associated with the height of the peak are much higher than that of the valley, which does not fit at all with the skewness values obtained.

These contradictory findings (also in section 3.1 with the original surfaces discussion) may be related to the fact that the methods used to obtain both volumetric and Abbott parameters are systematic and do not follow the same criteria. A good example is run #3, whose data is plotted in Figure 3.12.

Although they are different parameters, a qualitative comparative can be carried out. There is a significant difference in the position of the horizontal dotted lines that represent the boundaries that limit the peak, core and valley areas, even though it is the same accumulated height curve. This is also why neither of the two methods fits the discussion of the height distribution.

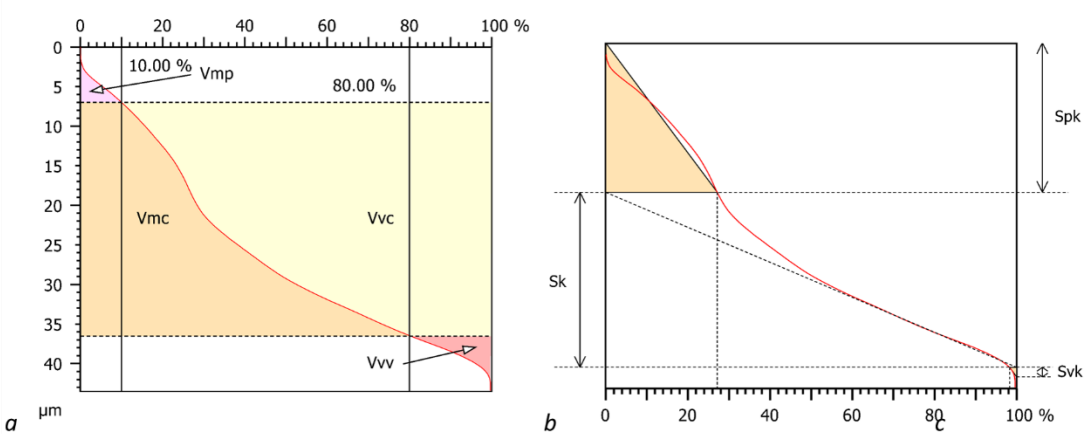

Figure 3.12. Accumulated height curve of run #3 VABB with a) volumetric parameters representation, and b) Abbott descriptors.

3.4. VABB vs. NVABB process

In order to assess the influence of the vibrations in the burnishing process, the S parameters that better represent the surface affectation are represented in Figure 3.13 for both processes, VABB and NVABB.

It shows close S_q values and similar trends for both processes. VABB only seems to perform better results in some cases for the first initial surface, so a pattern cannot be ruled for the influence of the process assisted by vibrations.

In general terms for the material redistribution, the Kurtosis values are also very close and all below 3. In none of the 54 runs performed, leptokurtic surfaces have been obtained. Regarding the skewness, very similar values are obtained for both processes, and generally, it is respected that a run is $S_{sk} > 0$ or $S_{sk} < 0$.

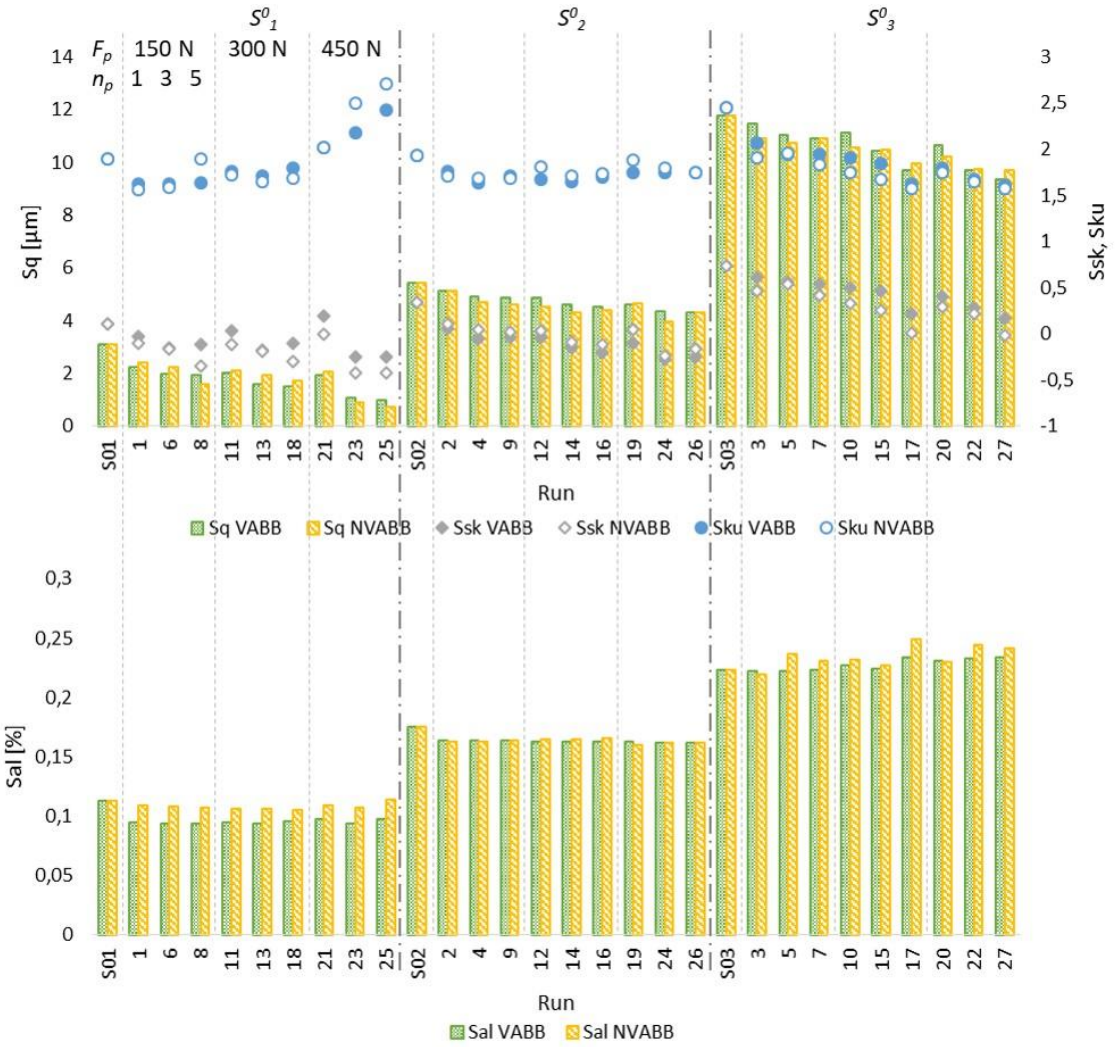

Figure 3.13. S_q, S_{sk} and S_{ku} comparative for VBB and NVABB processes.

Considering the S_{al}, each surface shows different behaviour. The smoother seems to be not affected when no vibrations are applied: the value keeps similar to the original, and in all cases above the VABB results. For the second surface, both VABB and NVABB show very similar tendency and values. And for the most abrupt one, a senseless fluctuation has been acquired. Almost all values show that S_{al} increases from the original surface so that the irregularities turn bigger.

Moreover, run #25 must be commented. Its S_q was the lowest value achieved by VABB, and now it has been further improved with NVABB. In addition, it has a closest S_{ku} to 3 than VABB, and S_{sk} approaches a little more to 0. This means that even the distribution shifts towards a slightly predominant presence of peaks, it still becomes narrower and closer to a perfect Gaussian distribution. This effect is confirmed with the histograms and 3D views shown in Figure 3.14.

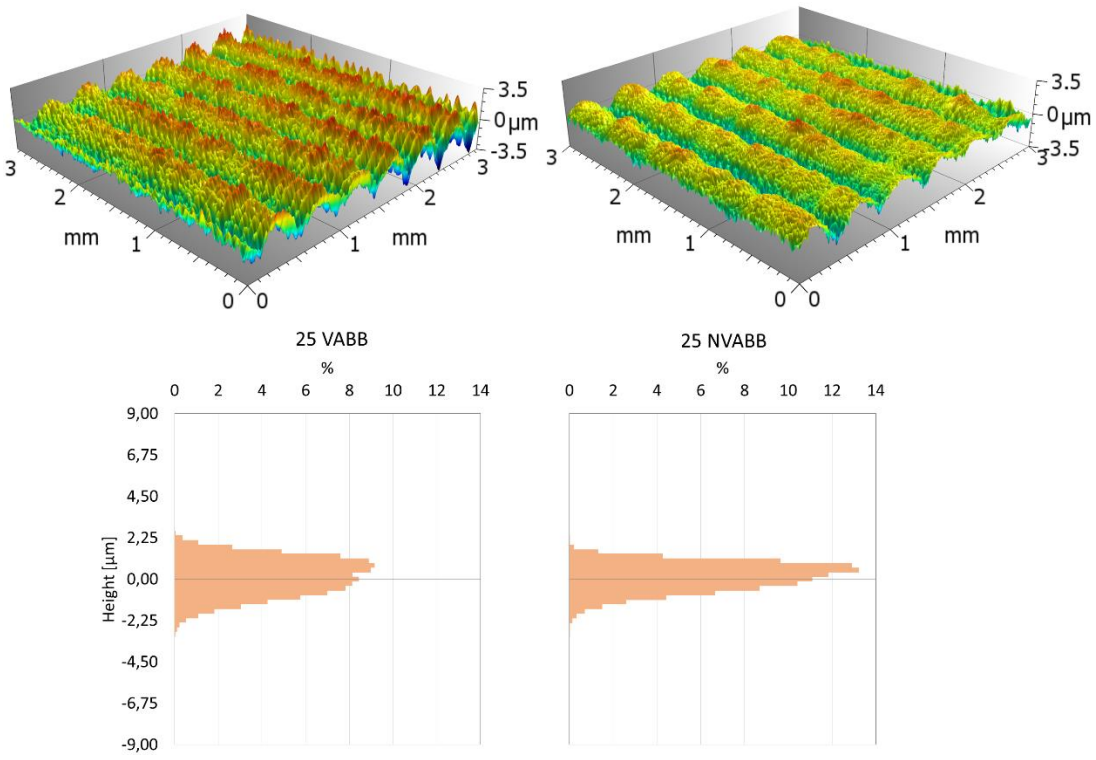

Figure 3.14. 3D views and accumulated height histogram comparison between run #25 VABB and NVABB.

Although the results obtained seem to point out that the vibration-assistance does not introduce a significant change in the surface texture, a visual inspection confirms that both processes do not have the same actual effect (3D views in Figure 3.14). It is evidenced together with the S_{al} values in the smoother surface. The VABB process has a higher interaction ball-surface that leads to more repeated surface irregularities in the peaks of the original milling pattern. So, the smoother the surface, the most sensitive to vibration-assistance.

These dissimilarities could highly affect the performance of the final parts. However, a further experimental investigation is needed to determine in which manner and how much the vibrations are decisive in the burnishing process.

4. Environmental impact analysis

This section is especially dedicated to the impact that may have to work with 720 nickel alloy on the environment. The aim is to qualitatively analyse the different stages in which the material is involved, from its manufacture to its life-time in-service conditions, to raise awareness of the high impact that conventional processes can entail.

The main process for obtaining nickel is pyrometallurgy, which is carried out in foundries at very high temperatures, which implies a high energy consumption and the emission of gases that can be toxic. Although the nickel itself can be recycled infinite times, the characteristics of a nickel-based superalloy after being formed make it difficult to be recycled. However, a few processes are available, but its high recycling process cost together with the small quantity of this material that is produced makes it technologically and economically not very feasible [31].

Nickel as an element is found abundantly in the earth's crust (0.008 %). Despite this, the mines that exploit it are mainly located in Canada, Russia and Central America [32]. Taking into account that the main aeronautic manufacturers are French and Americans, the supply chain entails a large expense and environmental impact on worldwide journeys.

As previously mentioned in this work, the 720 nickel alloy has also complex multi-phase heat treatment. The different stages could last up to 2 days, requiring high temperatures, which leads to the same case as in the foundries: high energy consumptions and the risk of toxic gas release.

Regarding the formation and manufacturing, the impact keeps rising. Although standard tooling methods are used for cold working, the usage of soft die materials is recommended to reduce the galling effect, which wears more easily. Besides, the heavy-duty lubricant may be used to extend the tooling life, while being very polluting [22]. After forming, it is also very important to remove all traces of the lubricant to prevent embrittlement at high temperatures, which could lead to a serious life reduction of the final part or catastrophic failure.

While every machining pass involves an additional expense in energy and wear of tools, adding the proper burnishing final process may lead to other benefits. Ensuring a good surface finish: lengthens the life of the part and the whole mechanism of which it is part by reducing the wear, enhances the fatigue life and prevents from debris accumulation. It is, a well-planned burnishing process that enhances the final part properties, allows to optimize its design and significantly lengthening its useful life, so it is not necessary to replace the part in advance with a new one. Moreover, it can also be further improved if the process is assisted by vibrations, allowing to reach the same level of improvement with fewer passes [13].

Regarding this project itself, all the machining operations where performed in the university laboratories. To collect all the remaining waste (material chip, lubricant, dirty paper, etc), the university has a special waste collection system consisting of five steps: identification and classification, packaging, labelling, storage, and collection process [33]. After the last step, the waste is delivered to the authorized manager in the legally established terms and conditions.

Apart from waste management, the carbon footprint of the energy consumption must also be taken into account: laboratory equipment, lightning, computers, and the internet.

Despite this, the improvements obtained from this line of research are expected to balance the environmental impact of the in-service conditions of the final pieces.

Conclusions

In this study, the effect of the ball-burnishing process assisted by vibrations has been analysed in the surface texture on 720 nickel alloy. Taking into account all the results obtained and the methods applied, the following conclusions are drawn from this work:

- Among the 5 variable factors analysed for the burnishing process, only the initial surface, preload, and the number of passes have a statistically significant influence on the surface height. There is no interaction between factors.
- It is possible to reduce the surface texture for the three initial surfaces throughout the work-hardening that causes the burnishing process, but only in S^0_1 does it evolve towards a unimodal distribution centred in the mean plane.
- Although there is not a big difference between S_q of 3 and 5 passes, it can make a difference when determining the distribution of the material.
- The run with the best results is #25 with the finest original surface, highest preload and 5 burnishing passes. As these conditions are limit levels for the three determining factors, the results may be further improved. More experiments may be performed with a new tool with higher preload limit, but other types of tests must be carried out to assess the surface or subsurface damage that the material may suffer due to excessive surface hardening compared to the bulk material.
- None of the runs has been reoriented in the burnishing preferential direction, so the net plastic deformation was not enough to erase the original milling pattern. Despite this, the second and third preferential directions have also been analysed. The finest surface shows an increasing presence of the burnishing path as the second preferential direction, for the higher preload.
- The Abbott curve and volumetric parameter sets are too subjective and dependent on the applied criterion and should not be decisive for the analysis.
- No differences are observed between the VABB and NVABB processes regarding the surface texture reduction and height redistribution, which show very similar numerical results. However, the vibrations-assisted process seems to interact more with the material surface, thus reducing significantly the irregularities scale in the smoother surface.

Future work

Due to the great interest of the industry in this line of research, all this work can be extended far beyond. For the moment, the analysis performed throughout this work has already been submitted for publication in Metals, a Q1 journal (in review).

Regarding the work ahead, these are the next steps to follow:

- Material characterization,
- Reconsider the levels of the factors, especially the preload in order to achieve greater plastic deformations,
- Complete the burnishing analysis through hardness, residual stresses, fatigue, and wear analysis, and
- Perform the test in a lathe to see how burnishing affects the properties in shafted-parts.

Economic analysis

This section contains a detailed economic analysis of the project expenses classified by categories:

MATERIAL AND MANUFACTURING			
Concept	Quantity	Cost per Unit	Total Cost
720 nickel alloy raw material (Ø 117 mm L 60 mm)	5 kg	150 €/kg	750,00 €
Machining and burnishing operations	300 €	1	300,00 €
		TOTAL	1.050,00 €

LABWARE AND SOFTWARE			
Concept	Quantity	Cost per Unit	Total Cost
STIL Stand Micromesure 2 & CCS Prima Optical Pen CL1-MG210 - Topographical sensor	30 h	30 €/h	900,00 €
SPIP 6.6.5 - Texture data post-processor	60 h	8 €/h	480,00 €
Minitab 19 software	30 h	0,52 €/h	15,60 €
MS Office software	240 h	0,08 €/h	19,20 €
		TOTAL	1.414,80 €

OTHER EXPENSES	
Concept	Total Cost
Laboratory use	500,00 €
Office supplies	40,00 €
TOTAL	540,00 €

ENGINEERING PROJECT			
Concept	Quantity	Cost per Unit	Total Cost
Project preparation	30 h	45 €/h	1.350,00 €
Performing of the experimental tests	30 h	45 €/h	1.350,00 €
Data acquisition	60 h	45 €/h	2.700,00 €
Results analysis	60 h	45 €/h	2.700,00 €
Drafting of the report	180 h	45 €/h	8.100,00 €
		TOTAL	16.200,00 €

SUPPORT ENGINEERING			
Concept	Quantity	Cost per Unit	Total Cost
Supervisor	20 h	70 €/h	1.400,00 €
Co-supervisor	20 h	70 €/h	1.400,00 €
External consultant	20 h	70 €/h	1.400,00 €
		TOTAL	4.200,00 €

TOTAL COST OF THE PROJECT	
Concept	Cost
Material and manufacturing	1.050,00 €
Labware and software	1.414,20 €
Other expenses	540,00 €
Engineering project	16.200,00 €
Support engineering	4.200,00 €
TOTAL	**23.404,80 €**

References

[1] N. H. Loh and S. C. Tam, "Effects of ball burnishing parameters on surface finish - A literature survey and discussion," *Precis. Eng.*, vol. 10, no. 4, pp. 215–220, 1988.

[2] R. L. Murthy and B. Kotiveerachari, "Burnishing of metallic surfaces - a review," *Precis. Eng.*, vol. 3, no. 3, pp. 172–179, 1981.

[3] A. Saldaña Robles, J. A. Diosdado de la Peña, A. de J. Balvantin García, E. Aguilera Gómez, H. Plasencia Mora, and N. Saldaña Robles, "El proceso de bruñido con bola: Estado del arte de una tecnología en desarrollo," *Dyna Ing. e Indrustria*, vol. 92, no. 1, pp. 28–33, 2017.

[4] B. Sachin, · S Narendranath, and · D Chakradhar, "Selection of optimal process parameters in sustainable diamond burnishing of 17-4 PH stainless steel," *J. Brazilian Soc. Mech. Sci. Eng.*, vol. 41, no. 3, p. 219, 2019, doi: 10.1007/s40430-019-1726-7.

[5] V. P. Kuznetsov, I. Y. Smolin, A. I. Dmitriev, S. Y. Tarasov, and V. G. Gorgots, "Toward control of subsurface strain accumulation in nanostructuring burnishing on thermostrengthened steel," *Surf. Coatings Technol.*, vol. 285, pp. 171–178, Jan. 2016, doi: 10.1016/j.surfcoat.2015.11.045.

[6] G. Rotella, S. Rinaldi, and L. Filice, "Roller burnishing of Ti6Al4V under different cooling/lubrication conditions and tool design: effects on surface integrity," *Int. J. Adv. Manuf. Technol.*, vol. 106, no. 1–2, pp. 431–440, Jan. 2020, doi: 10.1007/s00170-019-04631-z.

[7] H. Hamadache, M. Boubeira, O. Taamallah, and L. Laouar, "Surface hardening of 36 niCrMo 6 steel by ball burnishing process," *Mater. Res. Express*, vol. 6, no. 10, p. 106538, 2019.

[8] Z. Ding, J. Zhao, H. Liu, and Y. Dong, "Effects of ball burnishing on surface properties of SKD11 mold steel," 2020, doi: 10.1088/2631-8695/ab8443.

[9] R. J. Smith, G. J. Lewis, and D. H. Yates, "Development and application of nickel alloys in aerospace engineering," *Aircr. Eng. Aerosp. Technol.*, vol. 73, no. 2, pp. 138–146, 2001, doi: 10.1108/00022660110694995.

[10] "UDIMET alloy 720," vol. 106, no. Sept 04. Special Metals Corporation, 2004.

[11] R. Jerez-Mesa, J. A. Travieso-Rodriguez, G. Gomez-Gras, and J. Lluma-Fuentes, "Development, characterization and test of an ultrasonic vibration-assisted ball burnishing tool," *J. Mater. Process. Technol.*, vol. 257, pp. 203–212, Jul. 2018, doi: 10.1016/j.jmatprotec.2018.02.036.

[12] A. Estevez-Urra, J. Llumà, R. Jerez-Mesa, and J. A. Travieso-Rodriguez, "Monitoring of processing conditions of an ultrasonic vibration-assisted ball-burnishing process," *Sensors (Switzerland)*, vol. 20, no. 9, pp. 1–13, 2020, doi: 10.3390/s20092562.

[13] J. A. Travieso-Rodriguez *et al.*, "Effects of a ball-burnishing process assisted by vibrations in G10380 steel specimens," *Int. J. Adv. Manuf. Technol.*, vol. 81, no. 9–12, pp. 1757–1765, 2015, doi: 10.1007/s00170-015-7255-3.

[14] J. A. Travieso-Rodriguez *et al.*, "Experimental study on the mechanical effects of the vibration-assisted ball-burnishing process," *Mater. Manuf. Process.*, vol. 30, no. 12, pp. 1490–1497, 2015, doi: 10.1080/10426914.2015.1019114.

[15] R. Jerez-Mesa, Y. Landon, J. A. Travieso-Rodriguez, G. Dessein, J. Lluma-Fuentes, and V. Wagner, "Topological surface integrity modification of AISI 1038 alloy after vibration-assisted ball burnishing," *Surf. Coatings Technol.*, vol. 349, pp. 364–377, Sep. 2018, doi: 10.1016/j.surfcoat.2018.05.061.

[16] R. Jerez-Mesa, J. A. Travieso-Rodríguez, Y. Landon, G. Dessein, J. Lluma-Fuentes, and V. Wagner, "Comprehensive analysis of surface integrity modification of ball-end milled Ti-6Al-4V surfaces through vibration-assisted ball burnishing," *J. Mater. Process. Technol.*, vol. 267, pp. 230–240, May 2019, doi: 10.1016/j.jmatprotec.2018.12.022.

[17] J. V. López-Miralles, "Anàlisi topològic dels efectes del brunyit amb bola assistit per vibracions ultrasòniques," Universitat Politècnica de Catalunya, Barcelona, 2018.

[18] R. Jerez-Mesa, "Study and characterisation of surface integrity modification after ultrasonic vibration-assisted ball burnishing," Universitat Politècnica de Catalunya, 2018.

[19] I. Calliari, M. Magrini, and M. Dabalà, "Microstructural evolution of Udimet 720 superalloy," *J. Mater. Eng. Perform.*, vol. 8, no. 1, pp. 111–115, 1999, doi: 10.1361/105994999770347250.

[20] K. L. More and M. K. Miller, "Microstructural Characterization of UDIMET 720: a Nickel-Base Alloy," *J. Phys.*, vol. 49, no. 11, pp. 391–396, 1988, doi: 10.1051/jphyscol:1988667ï.

[21] H. Rodríguez Galbarro, "Ingemecanica.com," *Tutorial nº109: Propiedades del níquel y sus aleaciones*. [Online]. Available: https://ingemecanica.com/tutorialsemanal/tutorialn109.html. [Accessed: 19-Jun-2020].

[22] AZoMaterials, "Super Alloy Udimet 720 ™." AZoNetwork, pp. 2–5, 2013.

[23] W. P. Dong, P. J. Sullivan, and K. J. Stout, "Comprehensive study of parameters for characterizing three-dimensional surface topography I: Some inherent properties of parameter variation," *Wear*, vol. 159, no. 2, pp. 161–171, 1992, doi: 10.1016/0043-1648(92)90299-N.

[24] W. P. Dong, P. J. Sullivan, and K. J. Stout, "Comprehensive study of parameters for characterising three- dimensional surface topography. III: Parameters for characterising amplitude and some functional properties," *Wear*, vol. 178, no. 1–2, pp. 29–43, 1994, doi: 10.1016/0043-1648(94)90127-9.

[25] W. P. Dong, P. J. Sullivan, and K. J. Stout, "Comprehensive study of parameters for characterising three-dimensional surface topography. IV: Parameters for characterising spatial and hybrid properties," *Wear*, vol. 178, no. 1–2, pp. 45–60, 1994, doi: 10.1016/0043-1648(94)90128-7.

[26] E. S. Gadelmawla, M. M. Koura, T. M. A. Maksoud, I. M. Elewa, and H. H. Soliman, "Roughness parameters," *J. Mater. Process. Technol.*, vol. 123, no. 1, pp. 133–145, Apr. 2002, doi: 10.1016/S0924-0136(02)00060-2.

[27] E. J. Abbott and F. A. Firestone, "Specifying surface quality," *Mech. Eng.*, vol. 55, no. 569, 1933.

[28] G. Taguchi, S. Chowdhury, and Y. Wu, *Taguchi's Quality Engineering Handbook*. John Wiley & Sons, Inc., 2005.

[29] S. Marposs, "STIL Micromesure Sensors." [Online]. Available: http://micromesure.stil-sensors.com/. [Accessed: 21-Jun-2020].

[30] T. G. King and T. A. Spedding, "On the relationships between surface profile height parameters," *Wear*, vol. 83, no. 1, pp. 91–108, 1982, doi: 10.1016/0043-1648(82)90343-X.

[31] R. R. Srivastava, M. S. Kim, J. C. Lee, M. K. Jha, and B. S. Kim, "Resource recycling of superalloys and hydrometallurgical challenges," *J. Mater. Sci.*, vol. 49, no. 14, pp. 4671–4686, 2014, doi: 10.1007/s10853-014-8219-y.

[32] COMETAL, "Níquel." COMETAL, Madrid.

[33] UPC, "Laboratory Waste - Comunitat UPC Sostenible." [Online]. Available: https://sostenible.upc.edu/ca/recircula/recollida-selectiva/residus-de-laboratori. [Accessed: 01-Jun-2020].

Annexe A Surface parameters

This first annexe collects all the 3D S parameters used along with the work, where the following concepts must be considered form the work from Dong et al. (1994) [24]:

Equally spaced digitised 3D surface: $z(x_i, y_j)$ $(x_i = i\Delta x, y_j = j\Delta y; i = 1, 2, \dots, M; j = 1, 2, \dots, N)$, where Δx and Δy are the sampling intervals, and M and N represent the number of sampling points in the x and y directions, respectively.

All parameters are based on the residual surface, which is the difference between the original surface and the reference datum: $\eta(x_i, y_j) = z(x_i, y_j) - f(x_i, y_j)$

The residual surface has a zero mean: $\frac{1}{MN}\sum_{j=1}^{N}\sum_{i=1}^{M}\eta(x_i, y_j) = 0$

The five highest surface summits (peaks) and deepest pits (valleys) are, respectively, η_{si} $(i = 1, 2, \dots, 5)$ and η_{vi} $(i = 1, 2, \dots, 5)$.

t_x and t_y are the coordinates of the AACF (areal autocorrelation function analysis), that is the function that describes the general dependence of the values of the data at one position on the values at another position.

A1. S Amplitude parameters

$$S_a = \frac{1}{MN}\sum_{j=1}^{N}\sum_{i=1}^{M}|\eta(x_i, y_j)|$$ Average surface height

$$S_q = \sqrt{\left(\frac{1}{MN}\sum_{j=1}^{N}\sum_{i=1}^{M}\eta^2(x_i, y_j)\right)}$$ Root mean square height

$$S_{10z} = \frac{1}{5}\left(\sum_{k=1}^{5}|\eta_{si}| + \sum_{k=1}^{5}|\eta_{vi}|\right)$$ Ten-point height

$$S_{sk} = \frac{1}{MNS_q^3}\sum_{j=1}^{N}\sum_{i=1}^{M}\eta^3(x_i, y_j)$$ Skewness

$$S_{ku} = \frac{1}{MNS_q^4}\sum_{j=1}^{N}\sum_{i=1}^{M}\eta^4(x_i, y_j)$$ Kurtosis

A2. S Spatial parameter

$$S_{al} = \min\left\{\sqrt{t_x^2 + t_y^2}\right\} : AACF\left(t_x, t_y \leq 0.2\right)$$ Fastest decay autocorrelation length

A3. S Hybrid and Miscellaneous parameters

Root mean square gradient

$$S_{dq} = \sqrt{\frac{\sum_{j=4}^{N-3}\sum_{i=4}^{M-3}\left(\frac{\kappa(x_{i+1}, y_j) - \kappa(x_i, y_j)}{\Delta x}\right)^2 + \left(\frac{\kappa(x_i, y_{j+1}) - \kappa(x_i, y_j)}{\Delta y}\right)^2}{(N-6)(M-6)}}$$

Developed interfacial area ratio

$$S_{dr} = \frac{\sum_{j=1}^{N-1}\sum_{i=1}^{M-1}\sqrt{1 + \left(\frac{\kappa(x_{i+1}, y_j) - \kappa(x_i, y_j)}{\Delta x}\right)^2 + \left(\frac{\kappa(x_i, y_{j+1}) - \kappa(x_i, y_j)}{\Delta y}\right)^2}}{(N-1)(M-1)}$$

Texture direction

S_{td} Angle of texture's main direction

Annexe B L27 orthogonal matrix

The L27 orthogonal array developed by Taguchi [28] is capable of evaluating up to 13 factors at 3 levels with only 27 experiments. The 27 possible combinations of factors are shown in the table in subsection B1. It is also possible to analyse second-order influence if certain columns are left free: degrees of freedom. Three possibilities are available and are shown in the linear graphs in subsection B2.

B1. L27 Columns distribution

Run	Factors												
	1	2	3	4	5	6	7	8	9	10	11	12	13
1	1	1	1	1	1	1	1	1	1	1	1	1	1
2	1	1	1	1	2	2	2	2	2	2	2	2	2
3	1	1	1	1	3	3	3	3	3	3	3	3	3
4	1	2	2	2	1	1	1	2	2	2	3	3	3
5	1	2	2	2	2	2	2	3	3	3	1	1	1
6	1	2	2	2	3	3	3	1	1	1	2	2	2
7	1	3	3	3	1	1	1	3	3	3	2	2	2
8	1	3	3	3	2	2	2	1	1	1	3	3	3
9	1	3	3	3	3	3	3	2	2	2	1	1	1
10	2	1	2	3	1	2	3	1	2	3	1	2	3
11	2	1	2	3	2	3	1	2	3	1	2	3	1
12	2	1	2	3	3	1	2	3	1	2	3	1	2
13	2	2	3	1	1	2	3	2	3	1	3	1	2
14	2	2	3	1	2	3	1	3	1	2	1	2	3
15	2	2	3	1	3	1	2	1	2	3	2	3	1
16	2	3	1	2	1	2	3	3	1	2	2	3	1
17	2	3	1	2	2	3	1	1	2	3	3	1	2
18	2	3	1	2	3	1	2	2	3	1	1	2	3
19	3	1	3	2	1	3	2	1	3	2	1	3	2
20	3	1	3	2	2	1	3	2	1	3	2	1	3
21	3	1	3	2	3	2	1	3	2	1	3	2	1
22	3	2	1	3	1	3	2	2	1	3	3	2	1
23	3	2	1	3	2	1	3	3	2	1	1	3	2
24	3	2	1	3	3	2	1	1	3	2	2	1	3
25	3	3	2	1	1	3	2	3	2	1	2	1	3
26	3	3	2	1	2	1	3	1	3	2	3	2	1
27	3	3	2	1	3	2	1	2	1	3	1	3	2

B2. L27 Linear graphs

Linear graphical representation of the three possibilities (a, b, and c) for the arrangement of columns that allow evaluating second-order influences. In this study, option A has been chosen.

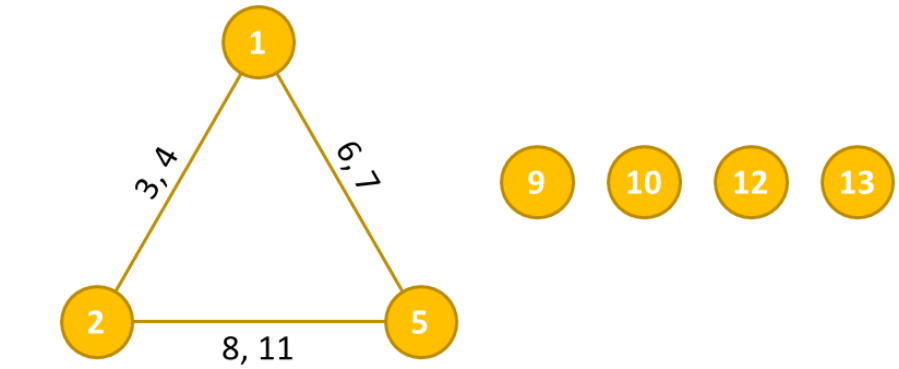

a

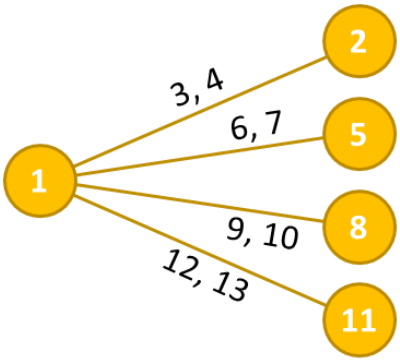

b

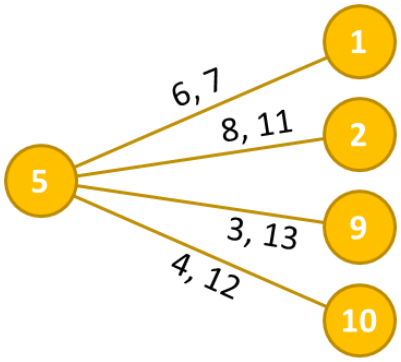

c

Annexe C Data report

It has been designed a report template in the post-processor software to collect in an organized way all the results obtained for each run. As an example, a general overview of the sections considered is shown here, for run 25 VABB:

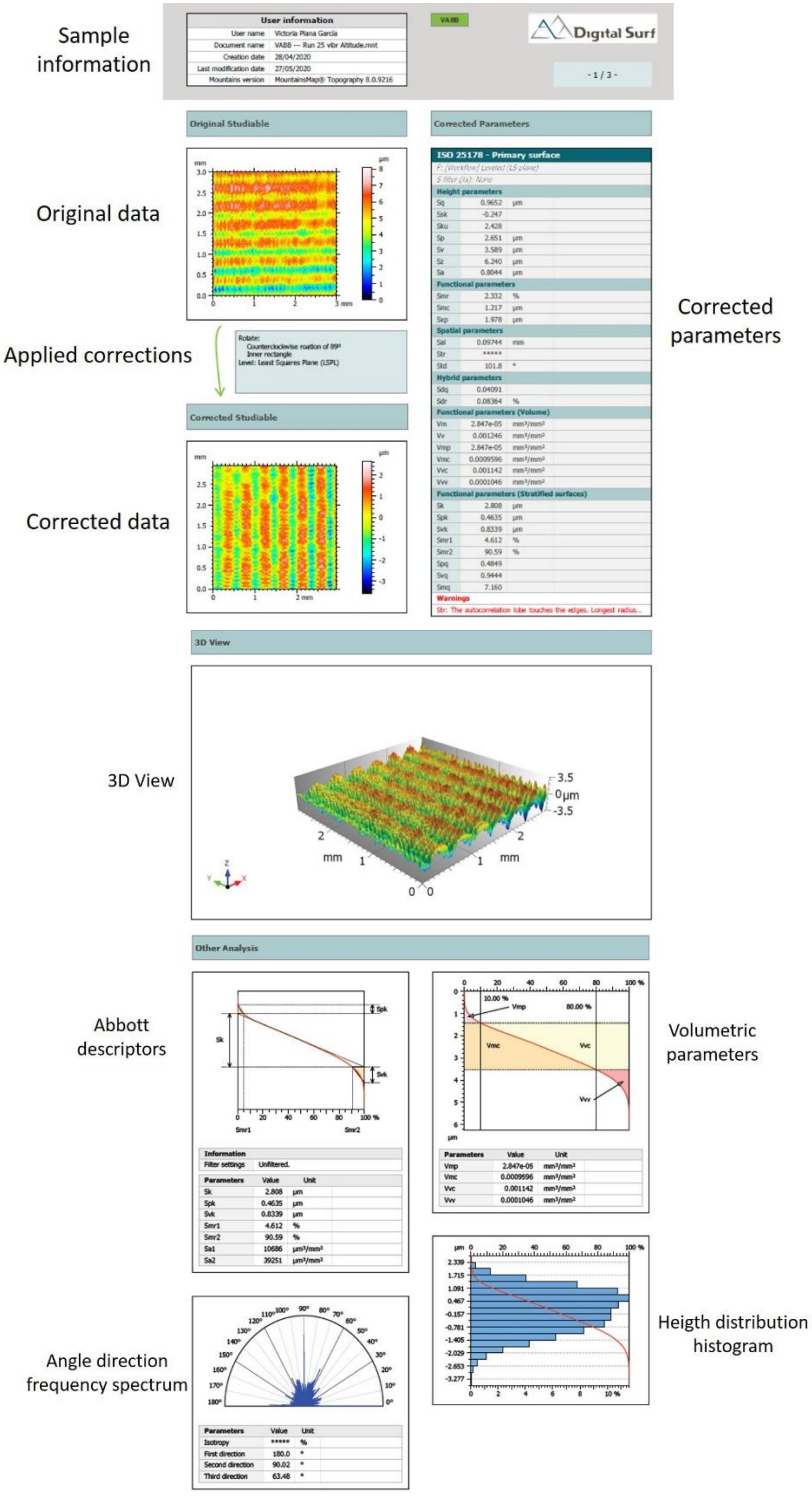

Annexe D Error correction with SPIP 6.6.5

Snapshots and sequence of commands for the software correction of outliers and void pixels that have been applied to correct the original data.

D1. Outliers correction

The sequence of commands followed to remove outliers in SPIP 6.6.5:

Image Tools > Modify > Filtering > Remove Outliers > Particles 99 %

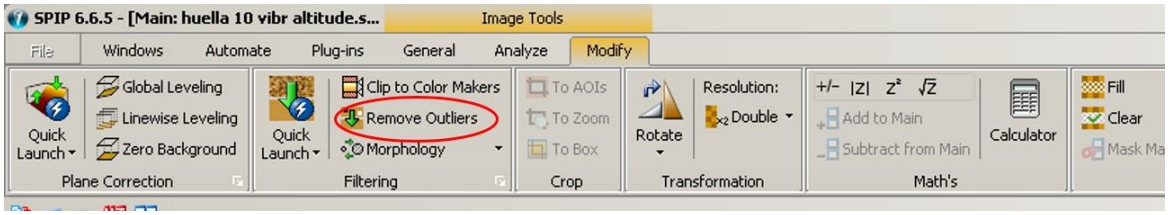

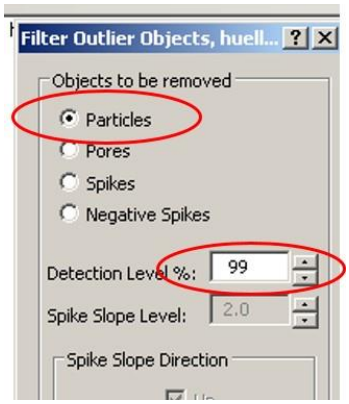

D2. White voids filling

The sequence of commands followed to fill the white voids in SPIP 6.6.5:

Image Tools > Modify > Void Pixels > Fill

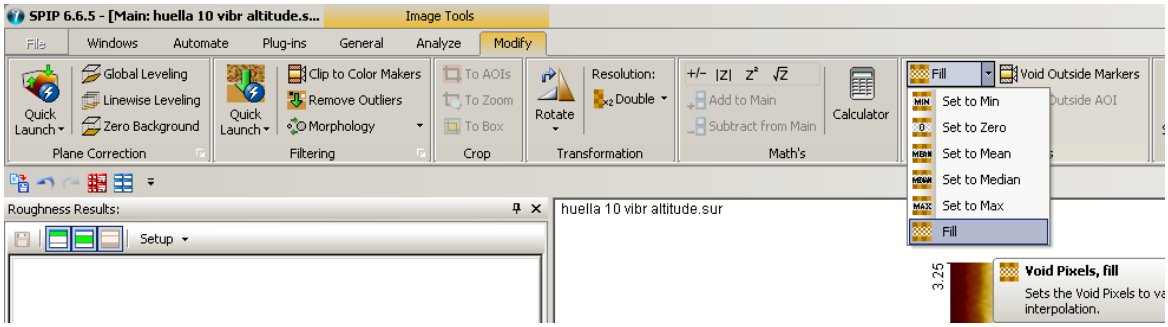

Annexe E S_a and S_q relationship

King and Spedding (1982) [30] found that the R_a and R_q 2D roughness parameters were proportional to each other. This relationship is a function of the skewness and kurtosis values and can also be applied for the 3D texture parameters S_a and S_q.

E1. Ratio R_a/R_q as a function of skewness and kurtosis [30]